iScience

CellPress
OPEN ACCESS

Article

Injectable Therapeutic Organoids Using Sacrificial Hydrogels

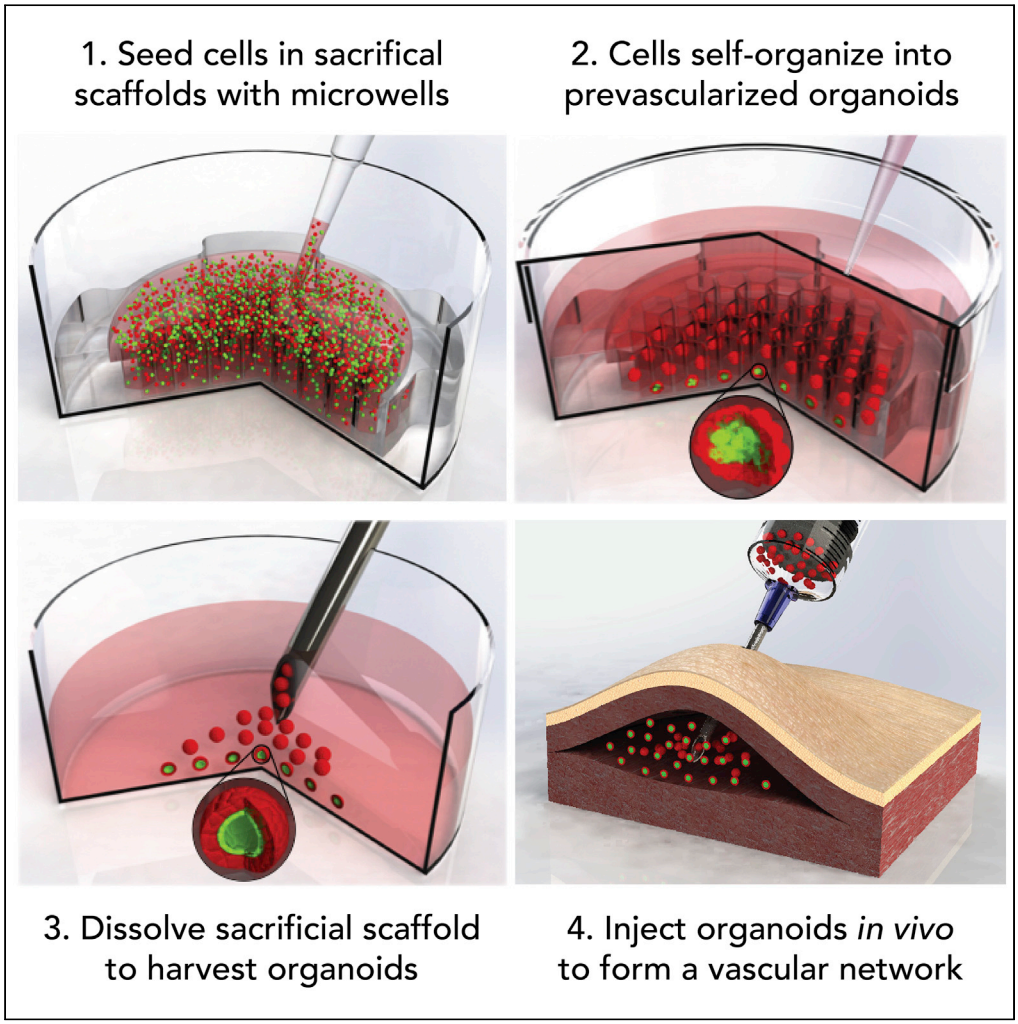

Ninna S. Rossen, Priya N. Anandakumaran, Rafael zur Nieden, ..., Danielle R. Bajakian, Brian M. Gillette, Samuel K. Sia

ss2735@columbia.edu

HIGHLIGHTS

Therapeutic, prevascularized organoids were formed in a sacrificial scaffold

The organoids are highly reproducible and grown in a high-throughput manner

The organoids rapidly formed perfusing vasculature in healthy mice

Therapeutic potential was assessed in a mouse model of peripheral artery disease

Rossen et al., iScience *23*, 101052
May 22, 2020
https://doi.org/10.1016/j.isci.2020.101052

iScience

CellPress
OPEN ACCESS

Article

Injectable Therapeutic Organoids Using Sacrificial Hydrogels

Ninna S. Rossen,[1,2,3,5] Priya N. Anandakumaran,[1,5] Rafael zur Nieden,[1,5] Kahmun Lo,[1] Wenjie Luo,[1] Christian Park,[1] Chuqiao Huyan,[1] Qinyouen Fu,[1] Ziwei Song,[1] Rajinder P. Singh-Moon,[1] Janice Chung,[1] Jennifer E. Goldenberg,[1] Nirali Sampat,[1] Tetsuhiro Harimoto,[1] Danielle R. Bajakian,[4] Brian M. Gillette,[1] and Samuel K. Sia[1,6,*]

SUMMARY

Organoids are becoming widespread in drug-screening technologies but have been used sparingly for cell therapy as current approaches for producing self-organized cell clusters lack scalability or reproducibility in size and cellular organization. We introduce a method of using hydrogels as sacrificial scaffolds, which allow cells to form self-organized clusters followed by gentle release, resulting in highly reproducible multicellular structures on a large scale. We demonstrated this strategy for endothelial cells and mesenchymal stem cells to self-organize into blood-vessel units, which were injected into mice, and rapidly formed perfusing vasculature. Moreover, in a mouse model of peripheral artery disease, intramuscular injections of blood-vessel units resulted in rapid restoration of vascular perfusion within seven days. As cell therapy transforms into a new class of therapeutic modality, this simple method—by making use of the dynamic nature of hydrogels—could offer high yields of self-organized multicellular aggregates with reproducible sizes and cellular architectures.

INTRODUCTION

Organoids, such as vascularized organoids or spheroids (de Moor et al., 2018; Wimmer et al., 2019, Mcguigan and Sefton, 2006), are three-dimensional multicellular clusters that mimic the structure and function of native tissues and are useful for on-chip drug screening (Alajati et al., 2008; Nam et al., 2015). For use as a cell therapy, delivery of cells within well-controlled microenvironments, rather than suspensions of isolated cells, could promote and maintain desired cellular functions within dynamic and complex *in vivo* environments (Takebe et al., 2013; Walser et al., 2013; Yap et al., 2013; Dissanayaka et al., 2014; Verseijden et al., 2010; Meyer et al., 2012). As organoids are increasingly being explored for *in vivo* studies and therapy, there is increasing recognition of the unmet challenge in generating multicellular aggregates with high reproducibility and control. As one example, even though control over "organoid size, shape, cellular composition and 3D architecture … is essential in order to understand the mechanisms that underlie organoid development in normal and pathological situations, and to use them as targets for manipulation or drug testing," reproducibility has been cited as "the major bottleneck of current organoid systems" (Huch et al., 2017).

The major current methods for generating organoids include spinner cultures (Sutherland et al., 1971), hanging drops (Tung et al., 2011; Frey et al., 2014), and non-adhesive 96-well plates (Ehsan et al., 2014; Yuhas et al., 1977; Metzger et al., 2011; Wenger et al., 2005) (Table S1), but these methods are difficult to scale or harsh to cells. (Alternatively, microtissues that are "cells in gels" (Chung and Park, 2009; Griffin et al., 2015; Huebsch et al., 2015; Li et al., 2014) typically feature cells moving to pre-formed pores within a hydrogel scaffold, but the cells are limited in their ability to self-organize into desired structures (Ovsianikov et al., 2018), and the resultant gels exhibit variable structures and sizes dependent on the pores and may be undesired in the implanted site due to potential immunogenicity.) More recently, methods to fabricate organoids based on micro-sized wells have faced challenges of either high adsorption (of steroid hormones, small molecules, and drugs (Li et al., 2009; Toepke and Beebe, 2006) for PDMS-based wells) or inefficient and harsh processes, usually involving vigorous pipetting or high-speed centrifugation, to separate and

[1]Department of Biomedical Engineering, Columbia University, 351 Engineering Terrace, 1210 Amsterdam Avenue, New York, NY 10027, USA

[2]Biotech Research & Innovation Centre, University of Copenhagen, University of Copenhagen, Ole MaaløesVej 5, 2200 Copenhagen N, Denmark

[3]Department of Radiation Oncology, Stanford University, 269 Campus Drive, Palo Alto, CA 94305, USA

[4]Department of Surgery - Division of Vascular Surgery and Endovascular Interventions, Columbia University Medical Center, Herbert Irving Pavilion, 161 Fort Washington Avenue, New York, NY 10032, USA

[5]These authors contributed equally

[6]Lead Contact

*Correspondence: ss2735@columbia.edu

https://doi.org/10.1016/j.isci.2020.101052

remove the cellular clusters from the microwells. Such procedures produce cellular clusters at a low yield and could damage cellular structures and function. Recognizing this limitation, other studies have proposed more complex methods to actively release cellular clusters from microwells (Shimizu et al., 2013; Tekin et al., 2010; Anada et al., 2010). As such, there still lacks reliable methods to generate organoids at high yield and with reproducibility and control over aggregate size and cellular organization.

Many hydrogels are biocompatible and have been used as a dynamically responsive biomaterial (such as microfluidic valve (Beebe et al., 2000), changing cellular microenvironment (Gillette et al., 2010), and stimuli-responsive drug release (Zhao et al., 2011)). We hypothesize that a dynamic change in the cross-linking state of hydrogels could gently release organoids and sought to demonstrate the strategy for producing large numbers of vascularized organoids to treat a mouse model of peripheral artery disease (Novosel et al., 2011; Dimmeler et al., 2014; Kim et al., 2016; Sun et al., 2016; Lovett et al., 2009), the most severe form of which is critical limb ischemia (CLI), which can lead to amputations (Davies, 2012). Thus far, attempts of cell therapy for treating CLI (including tens of clinical trials) have featured mesenchymal stem cells (MSCs) (Chen et al., 2008; Davies, 2012; Lawall et al., 2011; Raval and Losordo, 2013; Tongers et al., 2008) (which have not yet shown significant new re-perfusion) or endothelial cells (ECs) (which could die from prolonged deprivation of oxygen and nutrients before they form the desired blood vessels and anastomose with host vasculature (Benoit et al., 2013; Botham et al., 2013; Lawall et al., 2011)). We sought to demonstrate our approach to produce organoids with high reproducibility and scalability, as well as the ability to retain functionality after passing through needles to obviate invasive surgery (Kusamori et al., 2014; Lee et al., 2011; Mirabella et al., 2017) of ischemic sites with impaired wound healing. We also assessed the ability of the pre-formed blood-vessel units, after injection, to rapidly integrate with the host's vascular network in a healthy mouse model and to restore perfusion in an ischemic hindlimb mouse model.

RESULTS

Hydrogels as a Sacrificial Scaffold and as a Gentle and Scalable Method for Producing and Harvesting Organoids

Sacrificial materials are widely used in micromachining of microelectromechanical systems (MEMS) to release patterned metals or semiconductors from a substrate (Figure 1A). To cellular structures, some hydrogels (such as agarose or poly(ethylene)glycol as previously demonstrated) can be non-adhesive and thereby promote cells to interact with one another and contract into microtissues and organoids (de Moor et al., 2018; Lee et al., 2018). We hypothesized that a dynamic change in the cross-linking state of alginate, which can be achieved by adding calcium or a chelator and has been demonstrated for other purposes (Chen et al., 2017; Gillette et al., 2010, 2011; Wisdom et al., 2018) could similarly release cell-based structures from a surface without significantly disrupting the organoid structures or underlying cell function (Gillette et al., 2008). Specifically, we deposit the sacrificial material, create the sacrificial structure by cross-linking the alginate in its patterned state, deposit cells on top to allow cellular self-organization to take place, and remove the sacrificial layer by adding a chelator (5% w/v sodium citrate) (Figure 1A; see Figure S1 for fabrication details). The alginate is uncrosslinked within ~12 min (Figure 1B), to gently release a large number of organoids floating in solution (Figures 1C and 1D; Video S1). The resulting organoid solution could be gently pipetted into tubes, centrifuged and resuspended in a culture medium suitable for downstream manipulation or direct cell delivery. Each step is simple, can be conducted with sterile liquid handling, and can be automated.

The step of cellular self-organization can be adjusted depending on the organoid of interest. For vascularized organoids (Figure 1C), we seeded a co-culture containing ECs and MSCs (of either mouse or human origin) into the dissolvable alginate microwells. We cultured the cells in media without growth factors ("maintenance" medium) to induce cellular self-organization, followed by a vasculogenic medium with growth factors to induce cell-cell interactions including sprouting of blood-vessel-like structures. The organoids, now containing blood-vessel-like structures, are gently released by dissolving the alginate microwells.

The same small number of steps (Figures 1C and 1D) can harvest a large number of organoids by using alginate templates with large numbers of microwells. As an example, we demonstrated three different sizes of alginate microwell inserts for culture dishes (Figure 2A): 15.6-mm diameter inserts containing >1,000 microwells (yielding >24,000 organoids on a 24-well plate), 22.1-mm inserts containing >3,000 microwells (yielding >36,000 organoids on a 12-well plate), and a 60-mm diameter insert containing

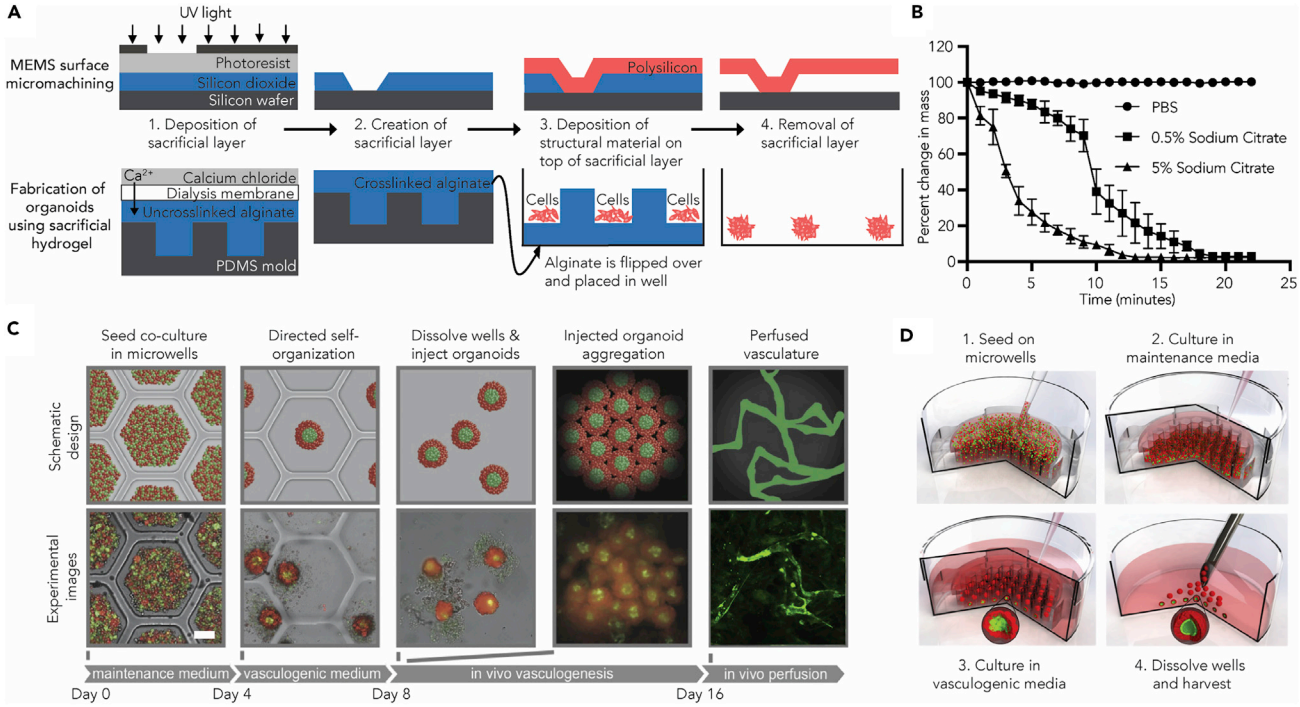

Figure 1. Schematic Diagram of Method of Using Sacrificial Hydrogels to Produce Therapeutic Organoids

(A) Schematic demonstrating the parallels between the surface micromachining method to fabricate MEMS devices such as a microcantilever (top) and the use of sacrificial alginate microwells to fabricate organoids (bottom). Both methods involve the use of a sacrificial layer (blue) to fabricate the final structure (red).

(B) Time required to completely uncrosslink alginate microwells following incubation with different concentrations of a chelator (sodium citrate) by measuring the percent change in mass over time (n = 3, data are represented as mean ± standard deviation).

(C) Schematic diagrams (top) and corresponding experimental images (bottom) showing the steps of organoid fabrication and *in vivo* perfusion. Experimental data were collected using GFP-labeled HUVECs and RFP-labeled mouse MSCs. First, a co-culture of endothelial cells (green) and mesenchymal stem cells (red) is seeded on dissolvable alginate microwells. Second, after being cultured in maintenance medium without growth factors for 3 to 4 days, cells self-organize into organoids with an endothelial core. A switch into culture medium with vasculogenic growth factors for an additional four days promoted formation of vessels within the organoids. Third, alginate microwells were dissolved with 5% sodium citrate to release organoids. Fourth, suspension of organoids could be centrifuged and assembled into a macro-tissue *in vitro* to study vascular formation or injected into the subdermis or ischemic hindlimb of a mouse to demonstrate engraftment *in vivo*. Fifth, injected organoids rapidly connected to form perfused microvasculature *in vivo*. Scale bar: 100 μm.

(D) The liquid handling steps in the process: (1) seeding the co-culture of ECs (green) and MSCs (red) by pipetting cells onto alginate microwell construct, (2) adding maintenance media once the cells have settled to the bottom of the microwells (approx. 30 minutes), (3) switching to vasculogenic media once an endothelial core has formed, and (4) gently dissolving the alginate microwells (approx. 12 minutes) to harvest organoids (the organoids can be gently washed prior to injection).

>30,000 microwells in a 60-mm culture dish. If desired, the inserts can be stacked to increase the number of organoids produced in the same area with additional media changes. Furthermore, the alginate microwells can be stored for up to one month (in the presence of 1.8 mM calcium chloride) without signs of degradation.

We demonstrated this massive parallel production of more than 30,000 organoids by seeding a quarter of a billion cells (Figure 2B) in one 60-mm dish insert (Figure 2C). We also tested the ability of the organoids to assemble *in vitro* into a macrotissue primed to form a microvascular network (Figure 2D). We co-cultured RFP-labeled MSCs and GFP-labeled ECs for four days, gently harvested the organoids, and assembled them into a macroscopic tissue with surface area of 1 cm^2 and a height of 1 mm (Figure 2D). We performed fluorescence imaging of this macroscopic tissue (Figure 2E). The organoids were densely packed, and exhibited distinct endothelial core structures, confirming that the gentle harvest and assembly did not disturb the internal architecture of the organoids. The assembled macrotissue, consisting of fully contracted organoids, did not visibly contract during subsequent *in vitro* culture.

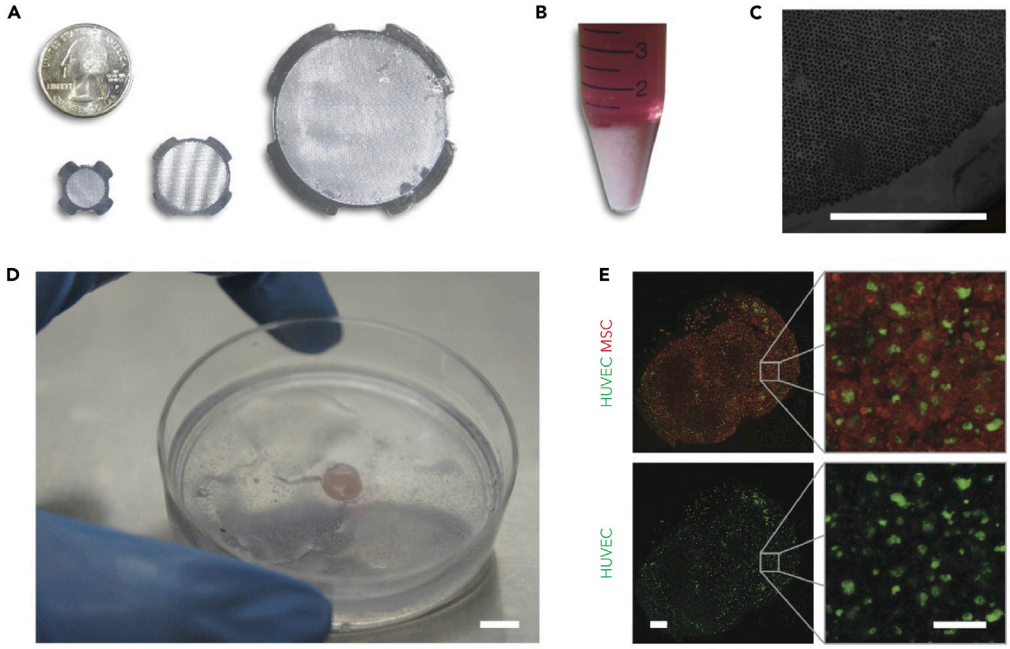

Figure 2. Production of Organoids at Large Scale and Functionality of Organoids to Form Macrotissue

(A) Pictures of three alginate microwells constructs for inserts into 24-well plates, 12-well plates, or 60-mm dishes with the capacity to produce 24 ×1,000; 12 ×3,000; or 30,000 organoids respectively.

(B) Picture of 250 million cells for seeding into alginate microwells. Cells in this figure are GFP-labeled HUVECs and RFP-labeled mouse MSCs.

(C) Stitched brightfield image of cells seeded in a 60-mm construct with 30,000 wells to create 30,000 organoids. Scale bar: 1 cm.

(D) Picture of a 1-mm-thick macrotissues with an area of 1 cm^2 assembled *in vitro* by collecting the 30,000 mature prevascularized organoids produced with the alginate microwell (A and B) construct in a 60-mm dish. Scale bar: 1 cm.

(E) Fluorescence images of the macrotissue in (D) with a close-up of the closely packed organoids with endothelial cores (green). Scale bars: 1 mm (left) and 500 μm (right).

Production of Organoids with Reproducible Size and Structure

Next, we studied whether the sizes and internal architectures of organoids could be controlled reproducibly. In the absence of exogenous growth factors, we observed that GFP-labeled human umbilical vein endothelial cells (HUVECs), which were initially randomly distributed alongside RFP-labeled mouse MSCs, migrate to the center of the organoids and form endothelial cores after culture in the "maintenance" medium for three days (Figure 3A, top panel, and Video S2). Similarly, ECs also formed endothelial cores when co-cultured with another cell type (fibroblasts) in a medium without growth factors (Figure S2), and the endothelial cores were more pronounced than in a previous observation (Wenger et al., 2005). By contrast, ECs did not migrate to the center when the organoids were initially cultured in a vasculogenic medium containing 40 ng/mL VEGF and 40 ng/mL bFGF (Figure 3A, bottom panel), consistent with a previous observation (Dissanayaka et al., 2014). Overall, the data showed the organoids to exhibit reproducible internal architectures containing endothelial cores.

We characterized the reproducibility of the method in controlling the size of the prevascularized organoid. By varying the microwell sizes and the co-culture ratios of cell types (Figure 3B), we controlled the number of cells that could aggregate into a single organoid. For example, microwells of three different sizes (100, 200, and 400 μm diameter) yielded organoids of three different sizes (39 ± 3 μm, 71 ± 5 μm, and 82 ± 7 μm diameter, respectively, all at the same cell-seeding concentration) (Figure 3B). The well size was chosen to be large enough to hold all the cells at the initial seeding concentration but small enough to ensure sufficient cell-cell contact to form a single organoid rather than multiple organoids. The cells aggregated into compact organoids within the first two days of *in vitro* culture, as seen by the decreasing radius of the smallest circle to include all cells (Figure 3C), with the main contraction happening in the first day and no further contraction after three days. The fully contracted organoids had a regular size distribution (Figure S3). We

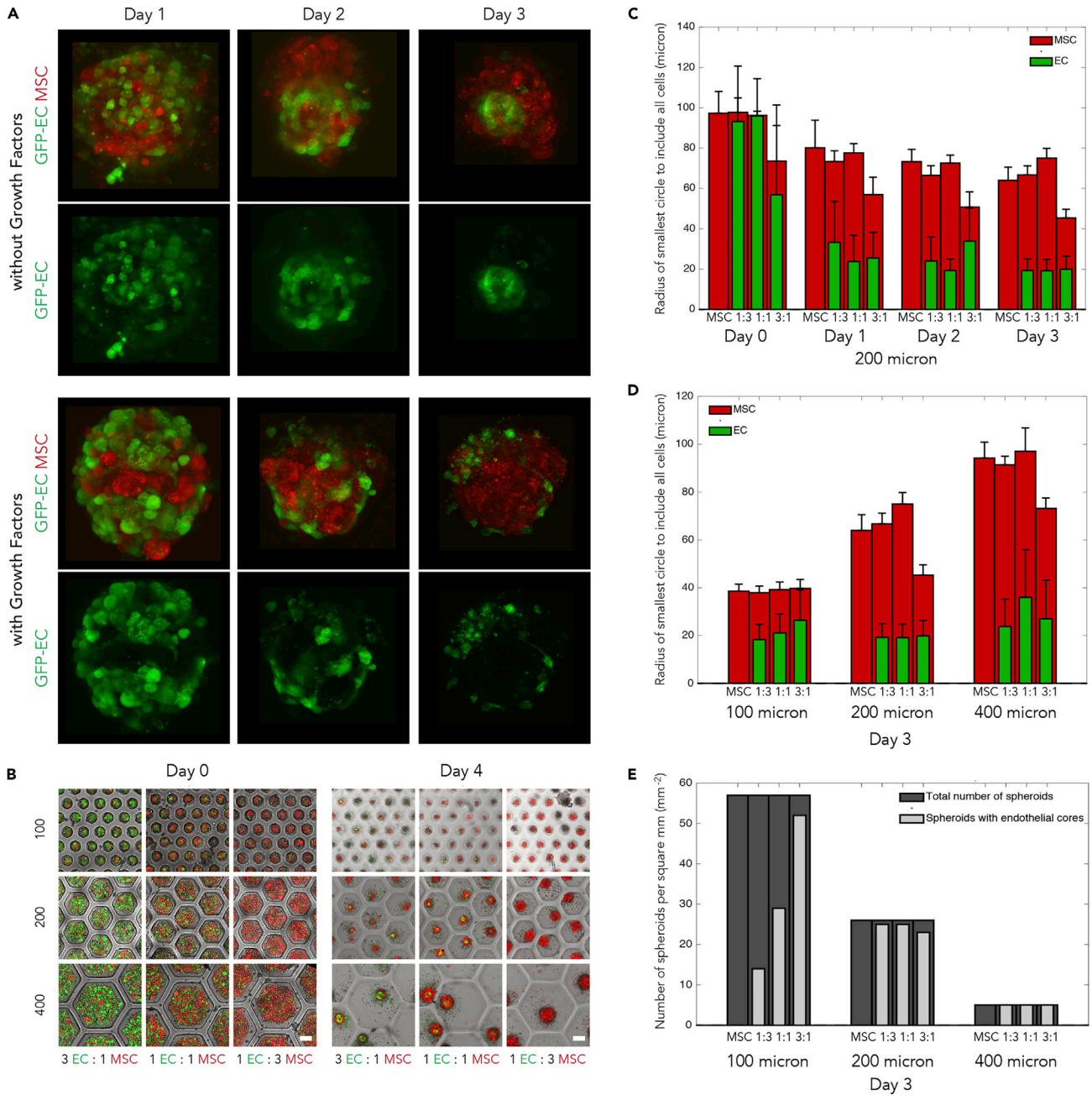

Figure 3. Production of Vascularized Organoids with High Reproducibility in Size and Structure

(A) Confocal fluorescence images of co-culture organoids of GFP-labeled HUVECs (green) and RFP-labeled mouse MSCs (red) over the first three days in maintenance medium without growth factors (top) or in vasculogenic medium with 40 ng/mL VEGF and 40 ng/mL bFGF (bottom). The cells self-organize by migration and either formed endothelial cores when cultured in media without growth factors (top) or had endothelial cells randomly distributed near the surface of the organoid and did not form endothelial cores when cultured in media with growth factors (bottom).

(B) Overlay of fluorescent and transmitted images showing parallel production of organoids in arrays of different sizes of microwells (with either 100, 200, or 400 μm diameter) and different co-culture ratios (1 EC: 3 MSC, 1 EC: 1 MSC, or 3 EC: 1 MSC). Different sizes of microwells yield different sizes of organoids, either unvascularized with only MSCs or prevascularized with a co-culture of ECs and MSCs, and different co-culture ratios yield different endothelial core sizes. Scale bar: 100 μm.

(C) Quantitative analysis of cell aggregation into organoids and the formation of an endothelial core over time in 200 μm microwells, as measured by the radius of the smallest circle that can contain all MSCs (red) or all ECs (green) ($n > 20$). Data are represented as mean ± standard deviation.

Figure 3. *Continued*

(D) Barplot showing the size of fully contracted organoids (red) and the size of the endothelial cores (green) for all tested microwell sizes and co-culture ratios. Data are represented as mean ± standard deviation.

(E) Reproducibility of endothelial cores; the number of organoids produced in 1 mm^2 (dark gray) and the number of organoids containing and endothelial core (light gray) for all tested microwell sizes and co-culture ratios.

See also Figures S2–S6.

also observed that the size of the fully contracted organoids (at day 2 and after) correlated to the number of cells in the organoid as expected; the diameter of the organoids' cross-sections related to the number of cells in the organoid and the cells' typical volume as $r_{organoid} = (6/\pi \cdot v_{cell} \cdot n_{cell})^{1/3}/2$ (Figure S4).

Also, we quantitatively analyzed the formation of organoids for cultures containing only MSCs and co-cultures with endothelial cell: mesenchymal stem cell (EC:MSC) ratios of 1:3, 1:1, and 3:1 (Figures 3B–3E). In 200-μm microwells, over three days, cells contracted into an organoid and ECs migrated toward the center (Figure 3C), and co-cultures in 400 μm microwells showed similar trends in organoid contraction and EC migration (Figure S5). Co-cultures in 100-μm microwells, however, did not contain enough cells (fewer than 150 cells in total) to form a distinct center (Figure S6). We also observed that the organoids per unit area and the number of organoids containing defined internal architectures could be controlled by varying microwell sizes and ratios of cell types (Figure 3E). (In subsequent *in vivo* studies, we have used 200-μm microwells with ratios of MSC only, 1 EC:3 MSC, and 1 EC:1 MSC, as these conditions showed aggregation involving almost all the cells within the microwells.) Overall, the data showed the method can produce organoids with internal architectures at high throughput and different sizes controllably.

Production of Prevascularized Human Organoids with Reproducible Size and Structure

We examined the effectiveness of this method for producing prevascularized organoids containing human adipose-derived MSCs (hAMSCs) with GFP-labeled human umbilical vein endothelial cells (HUVECs), in ratios of MSCs only, 1 EC:3 MSC, and 1 EC:1 MSC. We examined the maturation of organoids over eight days, where organoids were first grown in maintenance medium over three days to form endothelial cores, and then switched to vasculogenic medium containing exogenous growth factors for five days (Figure 4A). By day 8, vessel-like structures, such as lumens within the center of the organoid, with sprouting and maturation of vessels toward the surface were observed (especially evident in the larger organoids of the 400-μm wells). The initial migration of ECs was apparent after 20 h (Figures 4B and S7). In addition, we placed multiple prevascularized organoids inside 400-μm alginate wells that were collagen-doped, to mimic the adhesiveness of native tissues. Within 24 h, organoids attached to each other and contracted to form a larger, compact mesotissue (aggregation of multiple organoids) with a smooth outer border (Figure 4C, with additional time points in Figure S8 and Video S3). Hence, this method produced organoids containing human ECs and MSCs, with control over sizes and spatial architectures, and confirming the ability to form a prevascularized mesotissue.

Rapid Host Perfusion of Prevascularized Organoids in Mouse Model

Next, we assessed the effectiveness of the prevascularized organoids to self-organize to form a vascular network *in vivo*, anastomose to native host vasculature, and be perfused with host blood in a mouse model (Figure 5A). To facilitate real-time visualization, we performed surgery to place a window chamber (Figure S9) to permit brightfield, epifluorescence, and confocal imaging. We used organoids formed in 200-μm wells yielding organoids approximately 70 μm in diameter, which is also within the diffusion limit of oxygen (Lovett et al., 2009). We produced and harvested prevascularized organoids made of human cells (GFP-labeled HUVECs and hAMSCs), which we injected into SCID mice, a well-established animal model for studying integration of xenografts made of human cells (Steffens et al., 2009). We could inject and monitor the vascular formation for multiple different conditions (e.g., 1 HUVEC: 1 hAMSC and hAMSC only) in the same mouse, by utilizing the strong bond between the fascia and the subdermis. We injected the organoids through the fascia and into the space between the fascia and the subdermis, leaving the subcutaneous tissue intact between injection sites to create a barrier (Figure 5B). The organoids held up intact to the shear stress of injection through a syringe and needle (Figure S10). Interestingly, the shell of MSCs shielded the central blood-vessel building block against shear and preserved the organoids' architectural integrity after they passed through the needle. We also demonstrated the

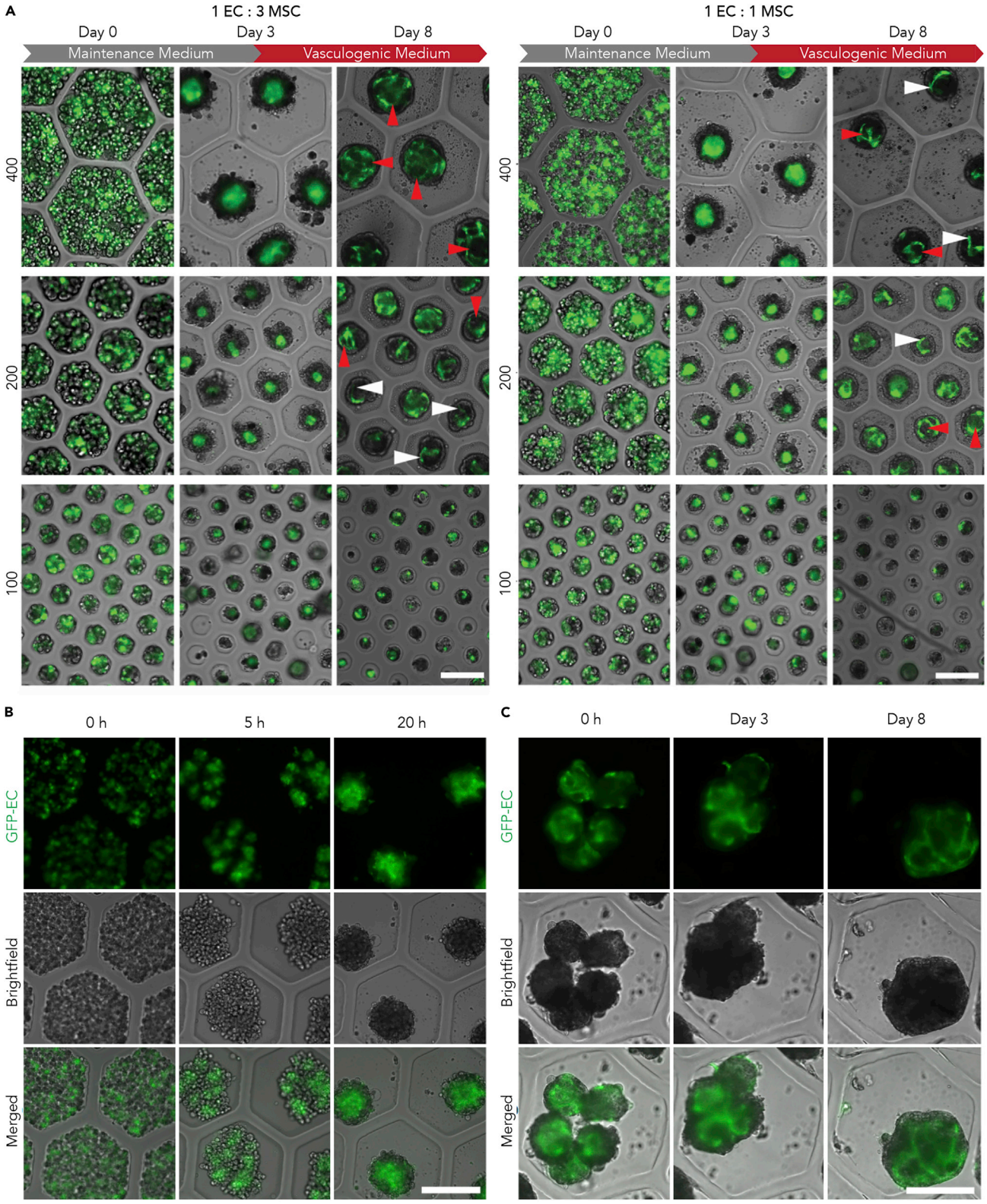

Figure 4. Production of Vascularized Organoids with Human Cells

(A) Maturation of endothelial cores with dynamic culture conditions for two co-culture ratios; 1 GFP-HUVEC: 3 hAMSC (left) and 1 GFP-HUVEC: 1 hAMSC (right). The cells are seeded (day 0) and initially cultured in maintenance medium without growth factors to form endothelial cores. After three days the

Figure 4. *Continued*
organoids were cultured in vasculogenic medium with 40 ng/mL VEGF and 40 ng/mL bFGF and the endothelial cores matured into vessels with discernable lumens (red arrows) and sprouts (white arrows). Scale bar: 200 μm.
(B) Epifluorescence, brightfield, and overlay images showing early self-organization of prevascularized organoids over the first 20 h, with a 1 GFP-HUVEC: 1 hAMSC co-culture in 400 μm microwells. Scale bar: 200 μm.
(C) Epifluorescence, brightfield, and overlay images showing fusion of prevascularized organoids (same conditions as in right A and B) into mesotissues over the first 24 h of the fusion process within a 400-μm collagen-doped alginate microwell. Scale bar: 200 μm.
See also Figures S7 and S8.

organoids could be injected directly into adipose tissue (Figure S11) and muscle tissue (Figure 6) with good integration.

We followed the formation of new vasculature by taking epiflourescent and stereoscopic images through the window chamber. Stereoscopic imaging (e.g., of the 1 HUVEC: 1 hAMSC conditions) showed vessel formation between day 4 and 7 (Figure 5B, top rows), with the implanted vasculature connecting to the host vasculature and becoming perfused (Figure 5B, top rows). After just seven days, host perfusion of the implanted vasculature was prominent and intense. The vessels were functional for the remaining 16 days of the 23-day *in vivo* studies. Quantitatively, we measured the length and number of the branched vessels and the total length of perfused vasculature in three regions of interest (ROIs) within the area of injected organoids (Figures 5C and S12). At day 7, areas injected with prevascularized organoids showed significant formation of new perfused vasculature, whereas areas injected with organoids consisting of MSCs only showed no increase in perfused vasculature (Figure 5B bottom row and Figure 5C). For all four mice tested (each with multiple conditions in the window chamber), all conditions with EC-containing organoids showed rapid vascularization of the injected organoids.

We also explored whether this self-organizing, "micro-to-macro" strategy could provide a limited but reproducible level of architectural control in the overall branching length of implanted, perfused microvasculature. Specifically, we hypothesized that average distances between endothelial cores could be related to diameters of organoids. The mean length of the perfused branches for 1 EC:1 MSC at day 7 was 93 $\pm$ 39 μm, with minimal changes by day 9–11, when the mean branch length was 86 $\pm$ 29 μm and 93 $\pm$ 44 μm, respectively (Figures 5D and S12). Indeed, the length of the newly formed vasculature's branches reflected the core-to-core distances between the densely packed, injected organoids with diameters of 71 $\pm$ 5 μm.

We also used epiflourescence and confocal microscopy to characterize the formation and integration of the new vasculature. Observing the GFP-labeled HUVECs through the window chamber (Figure 5E), we noticed the endothelial cores connecting with each other over time: the ECs initially appeared as discrete cores (day 0), then sprouted toward neighboring cores (day 4), connected with the host vasculature and became perfused (day 7), and stabilized as the perfused vascular network matured (day 9, 12, and 23). Between days 4 and 7, the network matured to form lumens (Figure 5E, red arrows). (We further confirmed the luminous structure of the newly formed, perfused network on day 11 via confocal microscopy on day 11; Video S4.) Moreover, we observed that areas indicating newly formed lumens (consisting of GFP-labeled HUVECs) co-localized with areas indicating host blood perfusion, further confirming that it was the newly formed luminous vasculature that was perfused, rather than angiogenesis from the host into the implanted tissue.

Rapid Re-vascularization and Restoration of Perfusion in a Hindlimb Ischemia Mouse Model

Finally, we assessed the effectiveness of this approach to treat ischemic conditions that are manifested in peripheral artery disease (PAD). We induced hindlimb ischemia by high femoral ligation with complete excision of the superficial femoral artery in C57BL/6 mice (Brenes et al., 2012) (Figure S13). We chose this surgical model because it consistently achieved reduced perfusion in the distal hindlimb but was more reproducible and better represented chronic manifestations of atherosclerotic disease than more severe hindlimb ischemia models, where all side branches were severed but resulted in less reproducible symptoms (Goto et al., 2006). We visualized and measured the perfusion of blood vessels close to the planar surface of the paw using laser speckle contrast imaging (LSCI) (Briers, 2001). Over a defined region, LSCI can image perfusion in microvasculature within 300 μm of the skin surface and provide accurate relative measurements of velocity of blood flow (Briers, 2001). Complete excision of the superficial femoral artery in the right hindlimb induced ischemia and limited perfusion, as confirmed by LSCI (Figure 6A, shown are days 1, 7, 9, and 14 post-ligation). In the saline-treated control group, the hindlimb recovered by approximately days 14–19 (Figures 6A and 6B), consistent with previous results for this femoral ligation model (Brenes et al., 2012).

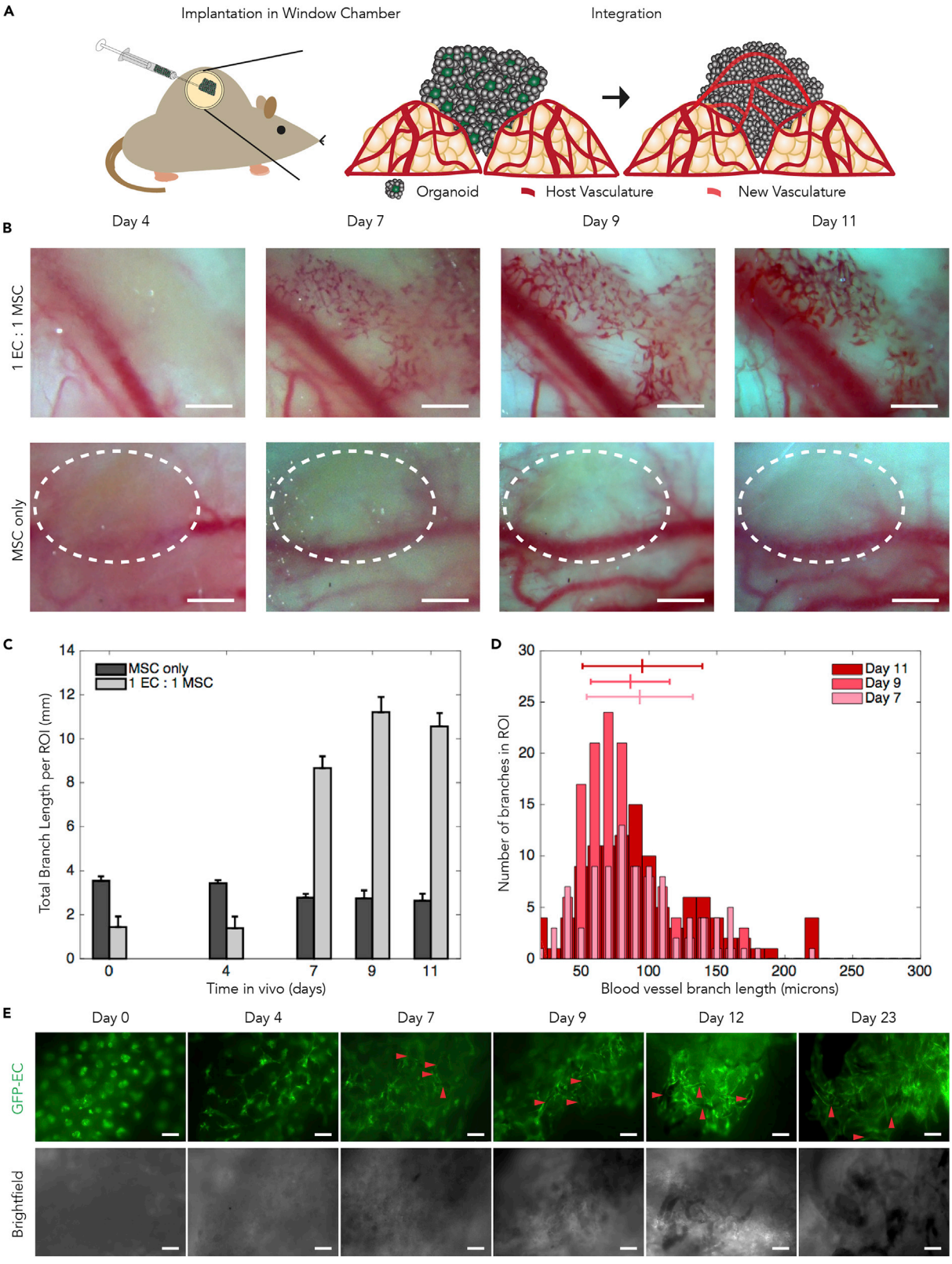
A
Implantation in Window Chamber
Integration
Organoid
Host Vasculature
New Vasculature
B
Day 4
Day 7
Day 9
Day 11
1 EC : 1 MSC
MSC only
C
MSC only
1 EC : 1 MSC
Total Branch Length per ROI (mm)
Time in vivo (days)
D
Day 11
Day 9
Day 7
Number of branches in ROI
Blood vessel branch length (microns)
E
Day 0
Day 4
Day 7
Day 9
Day 12
Day 23
GFP-EC
Brightfield

Figure 5. Rapid *In Vivo* Vascularization in Healthy Mice upon Injection of Organoids, as Observed in Real Time via a Window Chamber

(A) Schematic diagram of experimental setup for observing vascular formation and integration with host vasculature *in vivo* in real time via a window chamber. Organoids (from human cells formed under dynamic culture conditions in 200-μm microwells yielding organoids 71 ± 5 μm in diameter) were injected into a window chamber implant in an SCID mouse.

(B) Real-time *in vivo* stereoscopic images of prevascularized microtissues with 1 GFP-HUVEC: 1 hAMSC (top row) and unvascularized organoids with hAMSC only (bottom row) through window chamber at different time points. In the top row, newly formed vessels are apparent within 4 days, and blood-filled vessels observed by day 7. In the bottom row, the dashed white line indicates the area of organoids implant and no neo-vascularization was observed. Scale bar: 500μm.

(C) Quantification of neo-vascularization of the prevascularized organoids as the total length of vasculature within three ROIs of 800-by-800 μm containing up to 60 blood-filled vessel branches. The total length of vasculature increases substantially after day 7 for prevascularized organoids. There is no substantial difference in total length of the vasculature for the unvascularized organoids. Note that the blood-filled vessel intersections have been interpreted as branches and not as overpasses (which are two separate vessels, one over the other); however, further work is required to verify this. Data are represented as mean ± standard deviation.

(D) Distributions of branching length in the newly formed microvasculature (B and C) at day 7, 9, and 11. Lines above histogram indicate the mean branch length and standard deviation for day 7, day 9, and day 11 as 93 ± 39 μm, 86 ± 29 μm, and 93 ± 44 μm, respectively.

(E) Real-time *in vivo* images of prevascularized organoids with endothelial cells in green. The confining pressure of the intact fascia likely causes the spheroids to be organized in a two-dimensional grouping and was imaged at the plane of the endothelial cores. Red arrow heads point to luminous, blood-filled vessels (as indicated by dark lines in fluorescence images and dark areas of brightfield images). Scale bar: 250 μm.

See also Figures S9–S12.

For the cell-treatment group, we injected organoids into the hindlimb at four sites, taking advantage of the robustness of the organoids to shear stress (Figure S10) and thereby obviating invasive surgery (Mirabella et al., 2017). The organoids contained 2 million cells across the sites, in the range of previous studies (Brenes et al., 2012). Although mice in both the control and organoids groups exhibited a similar level of depressed perfusion in the injured hindlimb two days post-ligation, mice injected with organoids rapidly regained perfusion in the ischemic leg after 7 to 9 days (Figures 6A and 6B), a week quicker than the untreated control group.

Histological analysis of the gastrocnemius muscle from mice confirmed the ischemic limb of the control group displayed only few regenerating myofibers (Figure 6C), at levels indistinguishable from that of naive limbs (Figure 6D). Also, they showed signs of tissue necrosis, as indicated by a fragmented collection of short hypereosinophilic and swollen pale eosinophilic myofibers (Figure 6C). By contrast, histological cross-sections from mice injected with organoids showed centralized nuclei characteristic of regenerating myofibers (Figure 6C), with significantly more regenerating fibers than those of naive hindlimbs and ischemic limb of control group (Figure 6D). Moreover, cross-striations, which are characteristic of viable myofibers, were also more apparent in the hindlimbs of mice treated with organoids compared with control group (Figure 6D). The mice treated with injections of prevascularized organoids regained perfusion of the ischemic limb in just nine days, had more viable myofibers, and exhibited significantly more regenerating myofibers.

DISCUSSION

Using Sacrificial Hydrogels to Produce Organoids with High Reproducibility and Scalability

Like the development of micromachining techniques for producing MEMS structures reproducibly and on a large scale, we have developed a technique to use sacrificial hydrogels to produce clusters of self-organized cell-based structures with high reproducibility and scalability. Previously, we and other groups have shown the use of microfabricated hydrogels, including sacrificial techniques, to form *in vitro* microvascular networks (Gillette et al., 2008, 2010; Miller et al., 2012; Bertassoni et al., 2014). This paper demonstrates that the dynamic structure of hydrogels can also be exploited to produce and gently release organoids for cell therapy.

For purposes of cell therapy, it is critical for clinical efficacy, process control, and regulatory approval that cells introduced into the body are generated via tightly controlled processes and exhibit reproducible origin, size, and structure. Previous studies have observed that a "lack of control over the process is likely to underpin the variability in systems and experiments that, with few exceptions, does not allow [organoids] to yield their full potential," and the importance of achieving reproducible "organoid size, shape, cellular composition, and 3D architecture" in future research on organoids as well as use for therapeutic purposes (Huch et al., 2017). Compared with current organoid systems, our method can generate self-organized multicellular aggregates with both high yield (Table S1) and high reproducibility over aggregate size

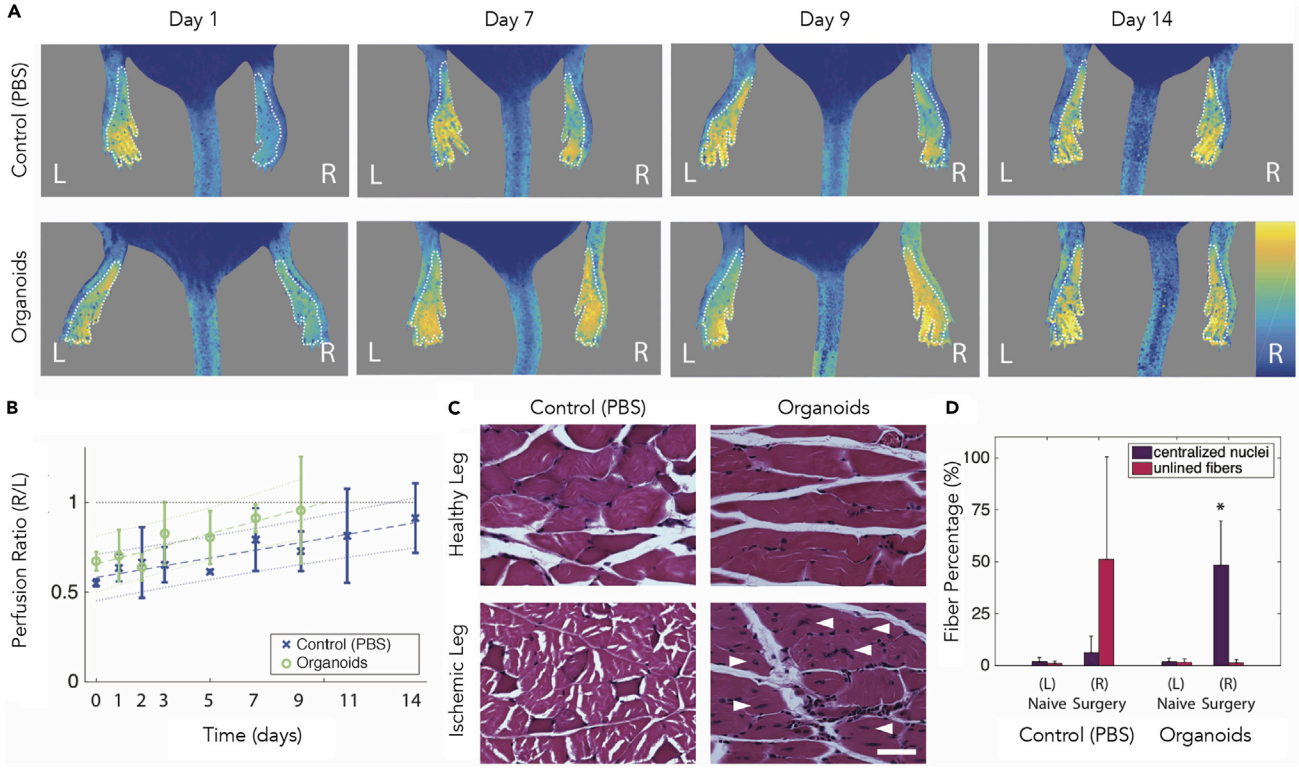

Figure 6. Rapid *In Vivo* Restoration of Perfusion and Muscle Fiber Regeneration upon Injection of Organoids in Ischemic Hindlimb

(A) Representative images of blood perfusion in the hindlimbs measured with laser speckle contrast imaging (LSCI) for the two experimental groups. The superficial femoral artery was isolated from the femoral vein and nerve bundle along the length of the thigh, ligated and excised. The mouse then received four injections along the length of the thigh of either 25 μL PBS (control) or organoids (corresponding to 0.5 × 10^6 cells) injected at each site. The organoids were formed in 200-μm microwells with maintenance media and a 1 mEC: 1 mMSC co-culture ratio yielding vascularized organoids 71 ± 5 μm in diameter with endothelial cores. The perfusion of each limb was measured as the average LSCI intensity of the planar surface of the paw (dashed white outline).

(B) Quantification of perfusion in the hindlimbs as the perfusion ratio (R/L) between the naive left (L) hindlimb and the ischemic right (R) hindlimb (n=3 mice for each condition) with the control mice in blue and the organoid treatment mice in green. Data are represented as mean ± standard deviation. The best-fit (dashed) and 95% confidence interval (dotted) lines are shown (from day 0–9 for organoids, from day 0–14 for control).

(C) Histology of the gastrocnemius muscle on day 14 with an H&E stain. White arrows indicate centralized nuclei of regenerating muscle fibers. Scale bar: 50 μm.

(D) Percentage of myofibers characterized as necrotic because of hyalinization (pink) or as regenerating, viable myofibers assessed by centralized nuclei (purple) (n=3).(4 ROIs of 587 × 440 μm^2 for each condition). Data are represented as mean ± standard deviation; * indicates significantly more regenerating fibers with $p < 0.05$.

See also Figures S10 and S13.

and cellular organization (Table S2). Moreover, the aggregate size and features of cellular organization can be tuned (Table S2), as our method bears similarities to MEMS fabrication technologies (in contrast to "cells in gels" systems that feature a distribution of pore sizes). In this study, sizes and internal architectures of the organoids were reproducible for different types of cells (MSCs and ECs of mouse and human origin), cell ratios, and overall size of microwells that determined the diameter of the contracted organoids. Even at the tissue level *in vivo*, branching lengths of the vascular network were reproducible (by contrast, microtissues with ECs had previously yielded non-uniform branching lengths (Ehsan et al., 2014; Rouwkema et al., 2006; Walser et al., 2013)).

Also, an ideal method for generating organoids should be scalable and gentle. In the common hanging-drop method, 384 organoids could be produced in the area of an overall standard well plate (with the overall scalability limited by the number of wells (Tung et al., 2011)), whereas the smallest construct shown in Figure 2 produces 24,000 organoids in the same area with fewer steps needed (e.g., media-changing steps, one alginate dissolving step), all of which could be automated by liquid

handling. The release of organoids is gentle even at a large scale, in contrast to vigorous pipetting or high-speed centrifugation for current microwell procedures. For cell therapy, it is important that the integrity of the cells be preserved (e.g., an FDA guidance document points to the need "to preserve integrity and function so that the products will work as they are intended" (Administration, 2017)). Beyond cell therapy, large-scale and effective production of organoids (beyond the quarter billion cells demonstrated) could also support studies in developmental biology, cancer cell intravasation (Ehsan et al., 2014), and organ printing.

An Advanced, Controlled Form of Cell Therapy for Disease Such as Ischemic Conditions

To date, more than 50 cell-therapy trials are at clinical stages for treating CLI. Many trials involve injecting MSCs (Davies, 2012; Tongers et al., 2008; Raval and Losordo, 2013; Lawall et al., 2011; Chen et al., 2008) or ECs (such as MarrowStim) (Lawall et al., 2011; Botham et al., 2013; Benoit et al., 2013), but the cells could die from deprivation of oxygen and nutrients before they are able to assemble into vascular networks *in vivo* and anastomose with host vasculature. In this study, after injection of organoids, we observed rapid revascularization and reperfusion (within 4–7 days in a mouse hindlimb ischemia model, compared with several weeks typical of implanted materials or tissues (Kang et al., 2016; Lokmic et al., 2007; White et al., 2014; Walser et al., 2013)), as well as low muscle necrosis. In a clinical scenario, such an approach could be especially attractive for "no-option" patients on the verge of amputation with subsequently poor mortality outcomes (60% within five years of surgery (Davies, 2012)).

In past studies, needle injection (and organ printing) with unilaminar vascular organoids (Fleming et al., 2010; Mironov et al., 2009) had been challenging due to shear stress formation. It would be advantageous in cell therapy to be able to deliver the cells via minimally invasive injection rather than invasive surgery. Our method produced organoids that held up intact to shear stress during injections, even with high-gauge (25–30) needles (Figure S10). This behavior may partially have been due to the shell of MSCs that protected the endothelial structure; interestingly, previous studies have also shown that the MSCs could act as an immune-suppressive shield for cell therapy in addition to providing angiogenic signaling (Huang et al., 2013; Iwase et al., 2005).

Limitations of the Study

Although we have demonstrated functionality of vascularized organoids composed of ECs and MSCs *in vivo* (even after minimally invasive injection through a needle), further *in vitro* work will be required to fully characterize and quantify the capillary-like vascular sprouts within the organoids. Not all combinations of ECs and other cells (including MSCs) may result in the endothelial core structures observed here, although the results of our method suggest cell-cell structures obtained will be reproducible. Moreover, before the vascularized organoids can be tested clinically, more work will have to be done to tailor dosages and study long-term preclinical outcomes compared with current cell therapy of suspensions of single cells. It will also be interesting to explore this technique as a platform for delivery of other types of stem and somatic cells, beyond those studied here.

METHODS

All methods can be found in the accompanying Transparent Methods supplemental file.

SUPPLEMENTAL INFORMATION

Supplemental Information can be found online at https://doi.org/10.1016/j.isci.2020.101052.

ACKNOWLEDGMENTS

We acknowledge technical assistance by Yaas Bigdeli and Ayse Karakecili and Mohammed Shaik and Elizabeth Hillman for help with imaging. We acknowledge funding from NIHR01HL095477-05R01 and NIH5R01HL141935. N.S.R. was supported by a fellowship from the Villum Foundation and Novo Nordisk Foundation Visiting Scholar Fellowship at Stanford Bio-X (NNF15OC0015218). R.z.N. was supported by the German National Academic Foundation, the Gerhard C. Starck Foundation, and the Klee Family Foundation.

AUTHOR CONTRIBUTIONS

N.S.R., R.z.N., B.M.G., and S.K.S. conceived the project and designed the experiments. N.S.R., P.N.A., R.z.N., K.L., W.L., C.P., C.H., Q.F., Z.S., R.P.S.-M., J.C., J.E.G., N.S., T.H., and B.M.G. conducted the experiments and analyses. N.S.R., P.N.A., R.z.N., and B.M.G. analyzed and interpreted the data. N.S.R., P.N.A., and R.z.N. prepared the figures, and N.S.R., R.z.N., and S.K.S. wrote the manuscript with contributions from P.N.A. and B.M.G., N.S.R., B.M.G., P.N.A., and S.K.S. supervised the project. All authors have reviewed the manuscript.

DECLARATION OF INTERESTS

A patent has been filed by Columbia University on the technology described in this study.

Received: January 26, 2020
Revised: March 11, 2020
Accepted: April 3, 2020
Published: May 22, 2020

REFERENCES

Administration, F.A.D. (2017). Regulatory considerations for human cells, tissues, and cellular and tissue-based products: minimal manipulation and homologous use; guidance for industry and food and drug administration staff; availability. Fed.Regist. *82*, 54290–54292.

Alajati, A., Laib, A.M., Weber, H., Boos, A.M., Bartol, A., Ikenberg, K., Korff, T., Zentgraf, H., Obodozie, C., Graeser, R., et al. (2008). Spheroid-based engineering of a human vasculature in mice. Nat. Methods *5*, 439–445.

Anada, T., Masuda, T., Honda, Y., Fukuda, J., Arai, F., Fukuda, T., and Suzuki, O. (2010). Three-dimensional cell culture device utilizing thin membrane deformation by decompression. Sens. Actuat. B Chem. *147*, 376–379.

Beebe, D.J., Moore, J.S., Bauer, J.M., Yu, Q., Liu, R.H., Devadoss, C., and Jo, B.-H. (2000). Functional hydrogel structures for autonomous flow control inside microfluidic channels. Nature *404*, 588.

Benoit, E., O'donnell, T.F., and Patel, A.N. (2013). Safety and efficacy of autologous cell therapy in critical limb ischemia: a systematic review. CellTranspl. *22*, 545–562.

Bertassoni, L.E., Cecconi, M., Manoharan, V., Nikkhah, M., Hjortnaes, J., Cristino, A.L., Barabaschi, G., Demarchi, D., Dokmeci, M.R., and Yang, Y. (2014). Hydrogel bioprintedmicrochannel networks for vascularization of tissue engineering constructs. Lab Chip *14*, 2202–2211.

Botham, C.M.B., Bennett, W.L., and Cooke, J.P. (2013). Clinical trials of adult stem cell therapy for peripheral artery disease. Methodist DebakeyCardiovasc. J. *9*, 201–205.

Brenes, R.A., Jadlowiec, C.C., Bear, M., Hashim, P., Protack, C.D., Li, X., LV, W., Collins, M.J., and Dardik, A. (2012). Toward a mouse model of hind limb ischemia to test therapeutic angiogenesis. J.Vasc.Surg. *56*, 1669–1679, discussion 1679.

Briers, J.D. (2001). Laser Doppler, speckle and related techniques for blood perfusion mapping and imaging. Physiol. Meas. *22*, R35–R66.

Chen, Y.X., Cain, B., and Soman, P. (2017). Gelatin methacrylate-alginate hydrogel with tunable viscoelastic properties. AIMS Mater. Sci. *4*, 363–369.

Chen, L., Tredget, E.E., Wu, P.Y., and Wu, Y. (2008). Paracrine factors of mesenchymal stem cells recruit macrophages and endothelial lineage cells and enhance wound healing. PLoS One *3*, e1886.

Chung, H.J., and Park, T.G. (2009). Injectable cellular aggregates prepared from biodegradable porous microspheres for adipose tissue engineering. Tissue Eng. Part A *15*, 1391–1400.

Davies, M. (2012). Critical limb ischemia: epidemiology. Methodist DebakeyCardiovasc. J. *8*, 10–14.

de Moor, L., Merovci, I., Baetens, S., Verstraeten, J., Kowalska, P., Krysko, D.V., de Vos, W.H., and Declercq, H. (2018). High-throughput fabrication of vascularized spheroids for bioprinting. Biofabrication *10*, 035009.

Dimmeler, S., Ding, S., Rando, T.A., and Trounson, A. (2014). Translational strategies and challenges in regenerative medicine. Nat. Med. *20*, 814–821.

Dissanayaka, W.L., Zhu, L., Hargreaves, K.M., Jin, L., and Zhang, C. (2014). Scaffold-free prevascularizedmicrotissue spheroids for pulp regeneration. J. Dent Res. *93*, 1296–1303.

Ehsan, S.M., Welch-Reardon, K.M., Waterman, M.L., Hughes, C.C., and George, S.C. (2014). A three-dimensional in vitro model of tumor cell intravasation. Integr.Biol. (Camb). *6*, 603–610.

Fleming, P.A., Argraves, W.S., Gentile, C., Neagu, A., Forgacs, G., and Drake, C.J. (2010). Fusion of uniluminal vascular spheroids: a model for assembly of blood vessels. Dev.Dyn. *239*, 398–406.

Frey, O., Misun, P.M., Fluri, D.A., Hengstler, J.G., and Hierlemann, A. (2014). Reconfigurable microfluidic hanging drop network for multi-tissue interaction and analysis. Nat. Commun. *5*, 4250.

Gillette, B.M., Jensen, J.A., Tang, B., Yang, G.J., Bazargan-Lari, A., Zhong, M., and Sia, S.K. (2008). In situ collagen assembly for integrating microfabricated three-dimensional cell-seeded matrices. Nat. Mater. *7*, 636–640.

Gillette, B.M., Jensen, J.A., Wang, M., Tchao, J., and Sia, S.K. (2010). Dynamic hydrogels: switching of 3D microenvironments using two-component naturally derived extracellular matrices. Adv. Mater. *22*, 686–691.

Gillette, B.M., Rossen, N.S., Das, N., Leong, D., Wang, M., Dugar, A., and Sia, S.K. (2011). Engineering extracellular matrix structure in 3D multiphase tissues. Biomaterials *32*, 8067–8076.

Goto, T., Fukuyama, N., Aki, A., Kanabuchi, K., Kimura, K., Taira, H., Tanaka, E., Wakana, N., Mori, H., and Inoue, H. (2006). Search for appropriate experimental methods to create stable hind-limb ischemia in mouse. Tokai J.Exp.Clin. Med. *20*, 128–132.

Griffin, D.R., Weaver, W.M., Scumpia, P.O., di Carlo, D., and Segura, T. (2015). Accelerated wound healing by injectable microporous gel scaffolds assembled from annealed building blocks. Nat. Mater. *14*, 737–744.

Huang, W.H., Chang, M.C., Tsai, K.S., Hung, M.C., Chen, H.L., and Hung, S.C. (2013). Mesenchymal stem cells promote growth and angiogenesis of tumors in mice. Oncogene *32*, 4343–4354.

Huch, M., Knoblich, J.A., Lutolf, M.P., and Martinez-Arias, A. (2017). The hope and the hype of organoid research. Development *144*, 938–941.

Huebsch, N., Lippens, E., Lee, K., Mehta, M., Koshy, S.T., Darnell, M.C., Desai, R.M., Madl, C.M., Xu, M., Zhao, X., et al. (2015). Matrix elasticity of void-forming hydrogels controls transplanted-stem-cell-mediated bone formation. Nat. Mater. *14*, 1269–1277.

Iwase, T., Nagaya, N., Fujii, T., Itoh, T., Murakami, S., Matsumoto, T., Kangawa, K., and Kitamura, S. (2005). Comparison of angiogenic potency between mesenchymal stem cells and

mononuclear cells in a rat model of hindlimb ischemia. Cardiovasc. Res. *66*, 543–551.

Kang, H.W., Lee, S.J., Ko, I.K., Kengla, C., Yoo, J.J., and Atala, A. (2016). A 3D bioprinting system to produce human-scale tissue constructs with structural integrity. Nat. Biotechnol. *34*, 312–319.

Kim, J.J., Hou, L., and Huang, N.F. (2016). Vascularization of three-dimensional engineered tissues for regenerative medicine applications. ActaBiomater. *41*, 17–26.

Kusamori, K., Nishikawa, M., Mizuno, N., Nishikawa, T., Masuzawa, A., Shimizu, K., Konishi, S., Takahashi, Y., and Takakura, Y. (2014). Transplantation of insulin-secreting multicellular spheroids for the treatment of type 1 diabetes in mice. J. Control Release *173*, 119–124.

Lawall, H., Bramlage, P., and Amann, B. (2011). Treatment of peripheral arterial disease using stem and progenitor cell therapy. J.Vasc.Surg. *53*, 445–453.

Lee, J., Sato, M., Kim, H., and Mochida, J. (2011). Transplantation of scaffold-free spheroids composed of synovium-derived cells and chondrocytes for the treatment of cartilage defects of the knee. Eur.CellMater. *22*, 90.

Lee, J.M., Yang, L., Kim, E.-J., Ahrberg, C.D., Lee, K.-B., and Chung, B.G. (2018). Generation of uniform-sized multicellular tumor spheroids using hydrogel microwells for advanced drug screening. Sci. Rep. *8*, 17145.

Li, N., Schwartz, M., and Ionescu-Zanetti, C. (2009). PDMS compound adsorption in context. J.Biomol.Screen *14*, 194–202.

Li, Y., Liu, W., Liu, F., Zeng, Y., Zuo, S., Feng, S., Qi, C., Wang, B., Yan, X., and Khademhosseini, A. (2014). Primed 3D injectable microniches enabling low-dosage cell therapy for critical limb ischemia. Proc. Natl. Acad. Sci. U S A *111*, 13511–13516.

Lokmic, Z., Stillaert, F., Morrison, W.A., Thompson, E.W., and Mitchell, G.M. (2007). An arteriovenous loop in a protected space generates a permanent, highly vascular, tissue-engineered construct. FASEB J. *21*, 511–522.

Lovett, M., Lee, K., Edwards, A., and Kaplan, D.L. (2009). Vascularization strategies for tissue engineering. Tissue Eng. Part B Rev. *15*, 353–370.

Mcguigan, A.P., and Sefton, M.V. (2006). Vascularized organoid engineered by modular assembly enables blood perfusion. Proc. Natl. Acad. Sci. U S A *103*, 11461–11466.

Metzger, W., Sossong, D., Bachle, A., Putz, N., Wennemuth, G., Pohlemann, T., and Oberringer, M. (2011). The liquid overlay technique is the key to formation of co-culture spheroids consisting of primary osteoblasts, fibroblasts and endothelial cells. Cytotherapy *13*, 1000–1012.

Meyer, U., Wiesmann, H.P., Libera, J., Depprich, R., Naujoks, C., and Handschel, J. (2012). Cartilage defect regeneration by ex vivo engineered autologous microtissue–preliminary results. In Vivo *26*, 251–257.

Miller, J.S., Stevens, K.R., Yang, M.T., Baker, B.M., Nguyen, D.-H.T., Cohen, D.M., Toro, E., Chen, A.A., Galie, P.A., and Yu, X. (2012). Rapid casting of patterned vascular networks for perfusable engineered three-dimensional tissues. Nat. Mater. *11*, 768.

Mirabella, T., Macarthur, J.W., Cheng, D., Ozaki, C.K., Woo, Y.J., Yang, M.T., and Chen, C.S. (2017). 3D-printed vascular networks direct therapeutic angiogenesis in ischaemia. Nat. Biomed.Eng. *1*, 0083.

Mironov, V., Visconti, R.P., Kasyanov, V., Forgacs, G., Drake, C.J., and Markwald, R.R. (2009). Organ printing: tissue spheroids as building blocks. Biomaterials *30*, 2164–2174.

Nam, K.H., Smith, A.S., Lone, S., Kwon, S., and Kim, D.H. (2015). Biomimetic 3D tissue models for advanced high-throughput drug screening. J. Lab. Autom. *20*, 201–215.

Novosel, E.C., Kleinhans, C., and Kluger, P.J. (2011). Vascularization is the key challenge in tissue engineering. Adv. Drug Deliv. Rev. *63*, 300–311.

Ovsianikov, A., Khademhosseini, A., and Mironov, V. (2018). The synergy of scaffold-based and scaffold-free tissue engineering strategies. Trends Biotechnol. *36*, 348–357.

Raval, Z., and Losordo, D.W. (2013). Cell therapy of peripheral arterial disease: from experimental findings to clinical trials. Circ. Res. *112*, 1288–1302.

Rouwkema, J., de Boer, J., and Van Blitterswijk, C.A. (2006). Endothelial cells assemble into a 3-dimensional prevascular network in a bone tissue engineering construct. Tissue Eng. *12*, 2685–2693.

Shimizu, K., Kusamori, K., Nishikawa, M., Mizuno, N., Nishikawa, T., Masuzawa, A., Katano, S., Takahashi, Y., Takakura, Y., and Konishi, S. (2013). Poly (N-isopropylacrylamide)-coated microwell arrays for construction and recovery of multicellular spheroids. J.Biosci.Bioeng. *115*, 695–699.

Steffens, L., Wenger, A., Stark, G.B., and Finkenzeller, G. (2009). In vivo engineering of a human vasculature for bone tissue engineering applications. J.Cell Mol. Med. *13*, 3380–3386.

Sun, X., Altalhi, W., and Nunes, S.S. (2016). Vascularization strategies of engineered tissues and their application in cardiac regeneration. Adv. Drug Deliv. Rev. *96*, 183–194.

Sutherland, R.M., Mccredie, J.A., and Inch, W.R. (1971). Growth of multicell spheroids in tissue culture as a model of nodular carcinomas. J.Natl. Cancer Inst. *46*, 113–120.

Takebe, T., Sekine, K., Enomura, M., Koike, H., Kimura, M., Ogaeri, T., Zhang, R.R., Ueno, Y., Zheng, Y.W., Koike, N., et al. (2013). Vascularized and functional human liver from an iPSC-derived organ bud transplant. Nature *499*, 481–484.

Tekin, H., Anaya, M., Brigham, M.D., Nauman, C., Langer, R., and Khademhosseini, A. (2010). Stimuli-responsive microwells for formation and retrieval of cell aggregates. Lab Chip *10*, 2411–2418.

Toepke, M.W., and Beebe, D.J. (2006). PDMS absorption of small molecules and consequences in microfluidic applications. Lab Chip *6*, 1484–1486.

Tongers, J., Roncalli, J.G., and Losordo, D.W. (2008). Therapeutic angiogenesis for critical limb ischemia: microvascular therapies coming of age. Circulation *118*, 9–16.

Tung, Y.C., Hsiao, A.Y., Allen, S.G., Torisawa, Y.S., Ho, M., and Takayama, S. (2011). High-throughput 3D spheroid culture and drug testing using a 384 hanging drop array. Analyst *136*, 473–478.

Verseijden, F., Posthumus-Van Sluijs, S.J., Farrell, E., van Neck, J.W., Hovius, S.E., Hofer, S.O., and van Osch, G.J. (2010). Prevascular structures promote vascularization in engineered human adipose tissue constructs upon implantation. CellTranspl. *19*, 1007–1020.

Walser, R., Metzger, W., Gorg, A., Pohlemann, T., Menger, M.D., and Laschke, M.W. (2013). Generation of co-culture spheroids as vascularisation units for bone tissue engineering. Eur.CellMater. *26*, 222–233.

Wenger, A., Kowalewski, N., Stahl, A., Mehlhorn, A.T., Schmal, H., Stark, G.B., and Finkenzeller, G. (2005). Development and characterization of a spheroidal coculture model of endothelial cells and fibroblasts for improving angiogenesis in tissue engineering. Cells Tissues Organs *181*, 80–88.

White, S.M., Pittman, C.R., Hingorani, R., Arora, R., Esipova, T.V., Vinogradov, S.A., Hughes, C.C., Choi, B., and George, S.C. (2014). Implanted cell-dense prevascularized tissues develop functional vasculature that supports reoxygenation after thrombosis. Tissue Eng. Part A *20*, 2316–2328.

Wimmer, R.A., Leopoldi, A., Aichinger, M., Wick, N., Hantusch, B., Novatchkova, M., Taubenschmid, J., Haemmerle, M., Esk, C., and Bagley, J.A. (2019). Human blood vessel organoids as a model of diabetic vasculopathy. Nature *565*, 505–510.

Wisdom, K.M., Adebowale, K., Chang, J., Lee, J.Y., Nam, S., Desai, R., Rossen, N.S., Rafat, M., West, R.B., Hodgson, L., and Chaudhuri, O. (2018). Matrix mechanical plasticity regulates cancer cell migration through confining microenvironments. Nat.Commun. *9*, 4144.

Yap, K.K., Dingle, A.M., Palmer, J.A., Dhillon, R.S., Lokmic, Z., Penington, A.J., Yeoh, G.C., Morrison, W.A., and Mitchell, G.M. (2013). Enhanced liver progenitor cell survival and differentiation in vivo by spheroid implantation in a vascularized tissue engineering chamber. Biomaterials *34*, 3992–4001.

Yuhas, J.M., Li, A.P., Martinez, A.O., and Ladman, A.J. (1977). A simplified method for production and growth of multicellular tumor spheroids. Cancer Res. *37*, 3639–3643.

Zhao, X., Kim, J., Cezar, C.A., Huebsch, N., Lee, K., Bouhadir, K., and Mooney, D.J. (2011). Active scaffolds for on-demand drug and cell delivery. Proc. Natl. Acad. Sci. U S A *108*, 67–72.

iScience, Volume *23*

Supplemental Information

Injectable Therapeutic Organoids

Using Sacrificial Hydrogels

Ninna S. Rossen, Priya N. Anandakumaran, Rafael zur Nieden, Kahmun Lo, Wenjie Luo, Christian Park, Chuqiao Huyan, Qinyouen Fu, Ziwei Song, Rajinder P. Singh-Moon, Janice Chung, Jennifer E. Goldenberg, Nirali Sampat, Tetsuhiro Harimoto, Danielle R. Bajakian, Brian M. Gillette, and Samuel K. Sia

SUPPLEMENTAL FIGURES

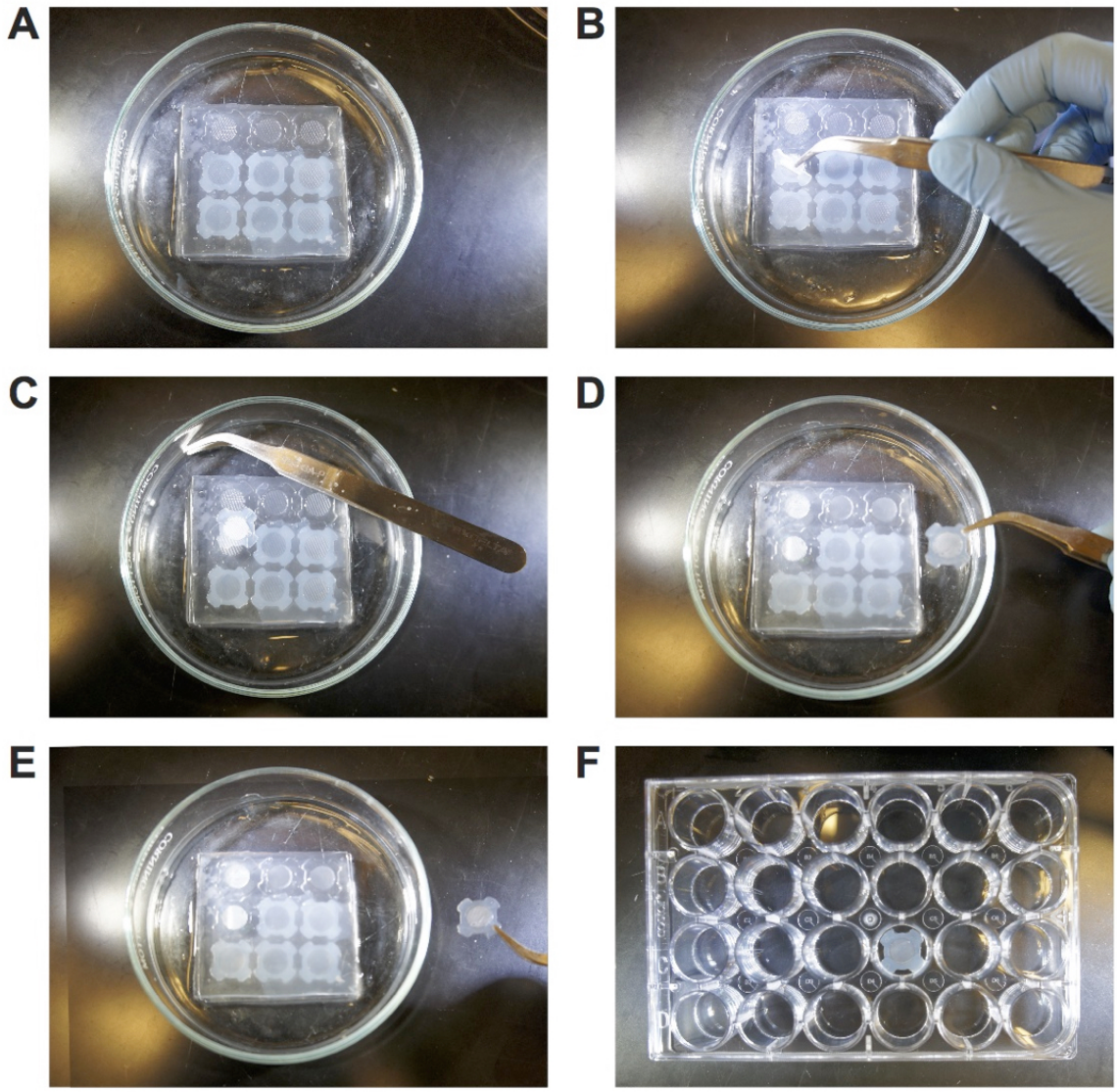

Figure S1. Fabrication of alginate-based micro-wells. Related to Figure 1. (A) shows six cross-linked alginate microwell constructs in the PDMS mold with the top three constructs removed. (B-D) The alginate molds are carefully loosened with a pair of sterile tweezers and removed from the mold holding on only to the "wings" to preserve the microwell structures in the middle. (E) The alginate constructs must be flipped to expose the microwells before being placed in the well plate (F).

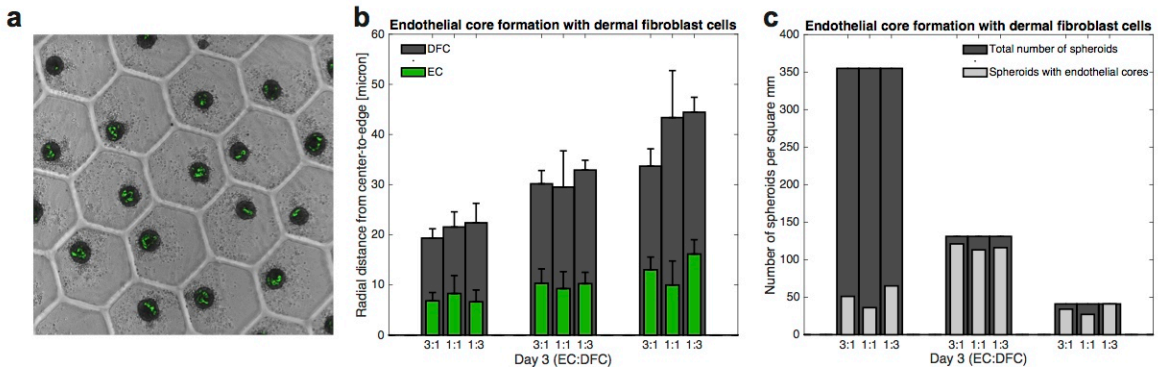

Figure S2. Endothelial core formation in co-culture with HUVECs and human dermal fibroblast cells (hDFCs). Related to Figure 3. (A) Image of organoid and endothelial core formation of 1 EC : 1 DFC in 400 µm wells after three days culture in maintenance medium. (B) Barplot of the radius of the smallest circle that can contain all ECs (green) or all DFCs (dark gray) for the different well sizes (100 µm, 200 µm, and 400 µm) at Day 3. (C) Barplot of the number of organoids/spheroids formed per mm^2 (dark grey) in 100 µm, 200 µm, and 400 µm wells and the number of those organoids that contain endothelial cores (light grey).

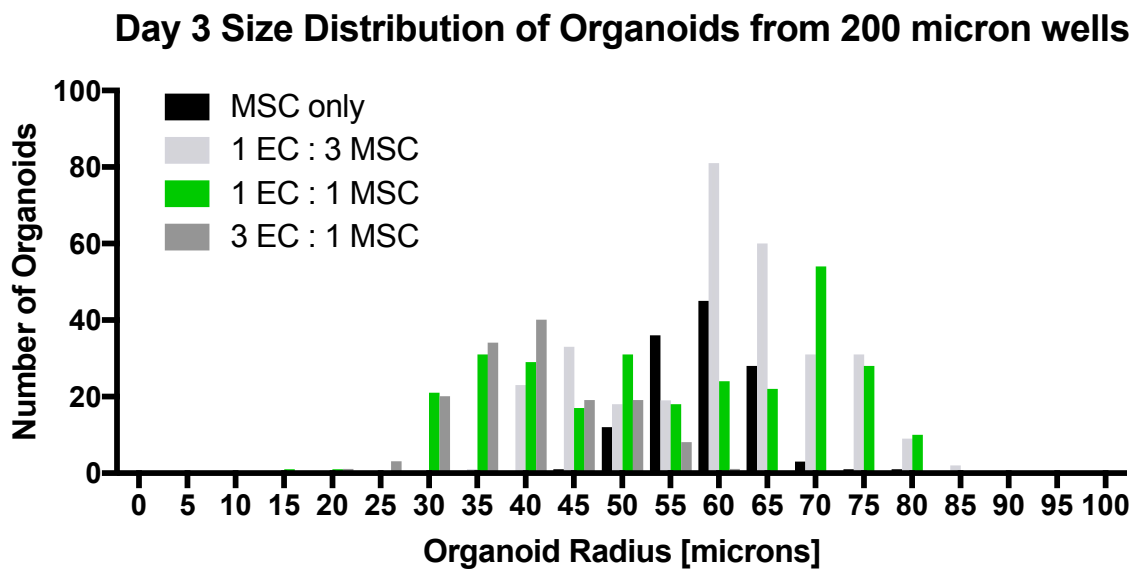

Figure S3. Size distribution of the organoids formed in 200 μm wells. Related to Figure 3. MSC only (black) and 1 EC : 1 MSC (green) organoids were used in the *in vivo* studies in Fig. 5 and Fig. 6.

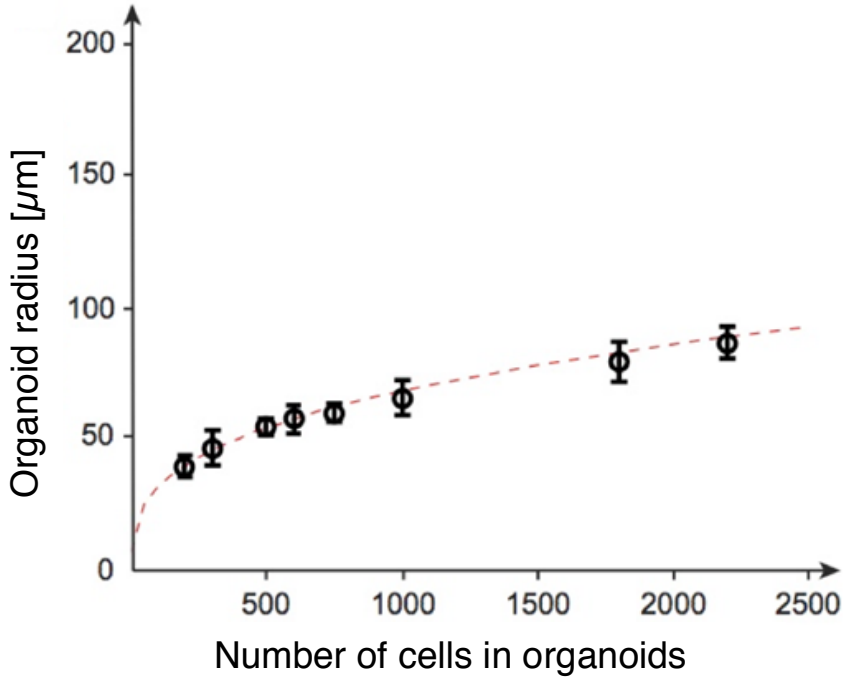

Figure S4. Organoid size is a function of the number of cells inside. Related to Figure 3. Our method provides two mechanisms to control the number of cells in each organoid; either by changing the size of alginate wells or by changing the seeding cell density. Utilizing both, we got organoids with 200, 300, 500, 600, 750, 1000, 1800, and 2200 cells. The radius of the resulting, fully-aggregated organoids after 3 days follows the expected equation $r_{organoid} = (6/\pi\ v_{cell}\ n_{cell})^{1/3}/2$.

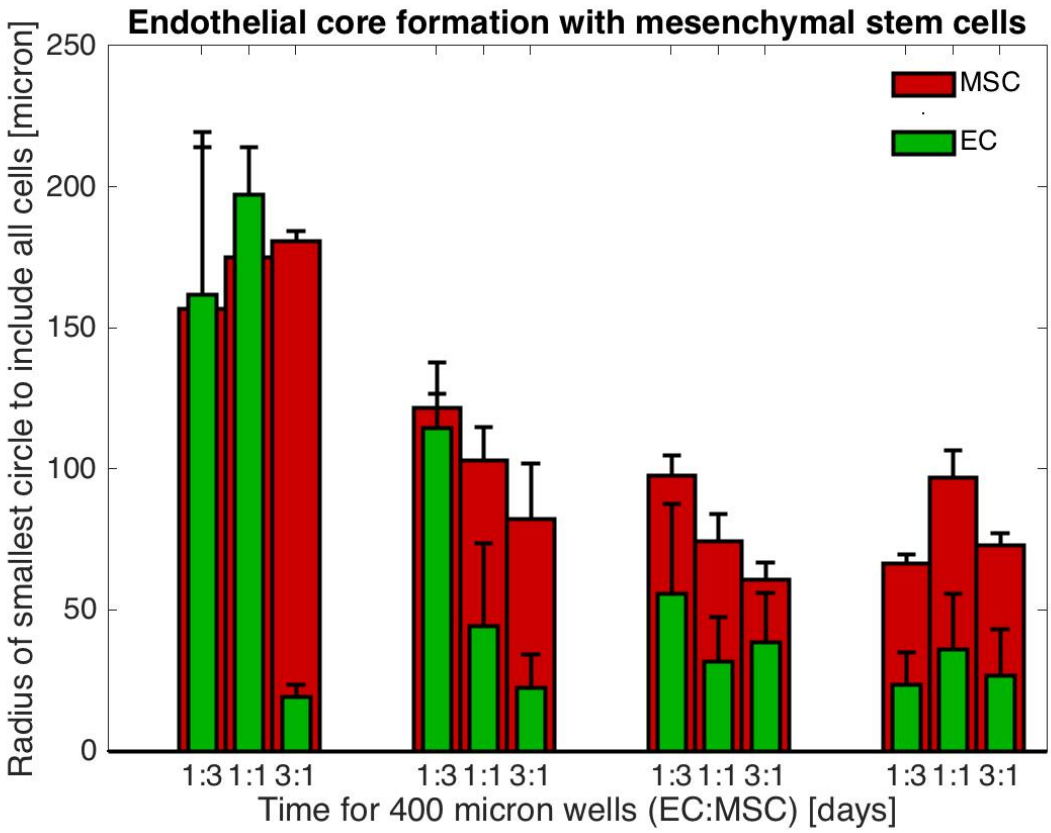

Figure S5. Organoid contraction and endothelial core formation in 400-micron microwells from day 0 to day 3. Related to Figure 3.

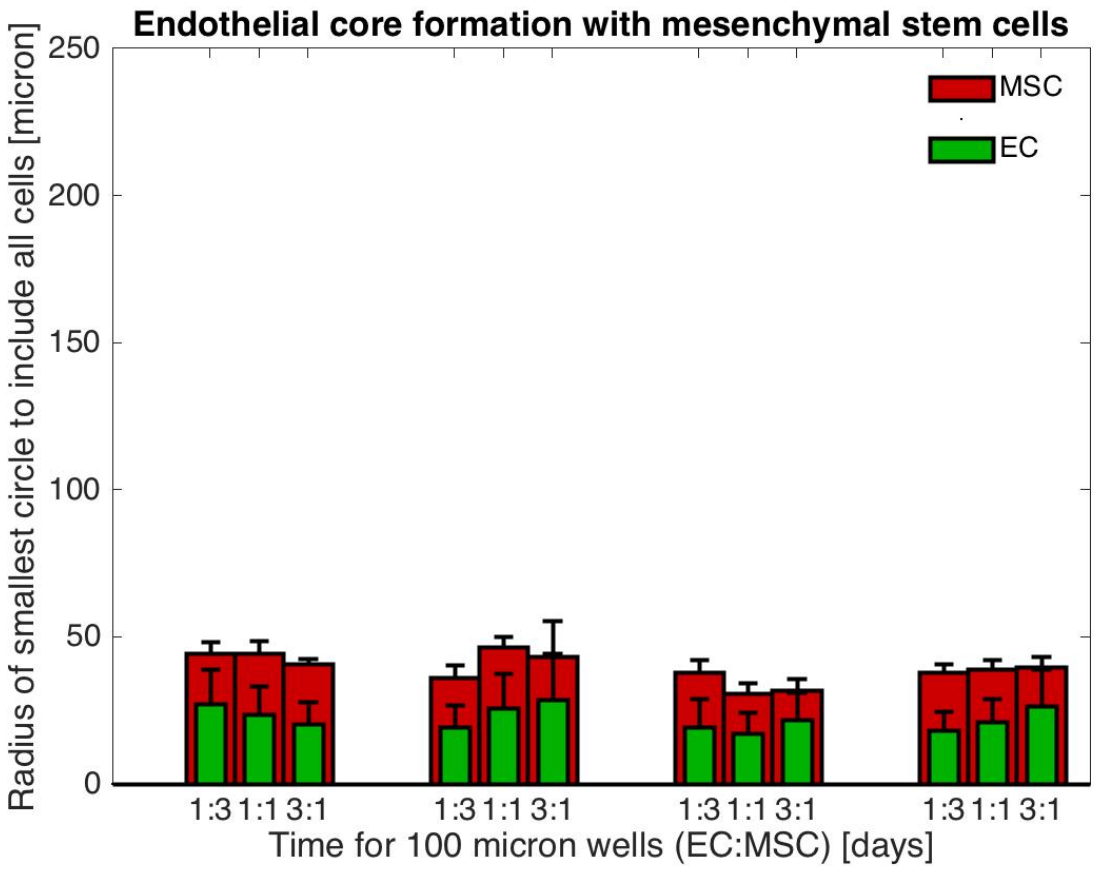

Figure S6. Organoid contraction and endothelial core formation in 100-micron microwells from day 0 to day 3. Related to Figure 3.

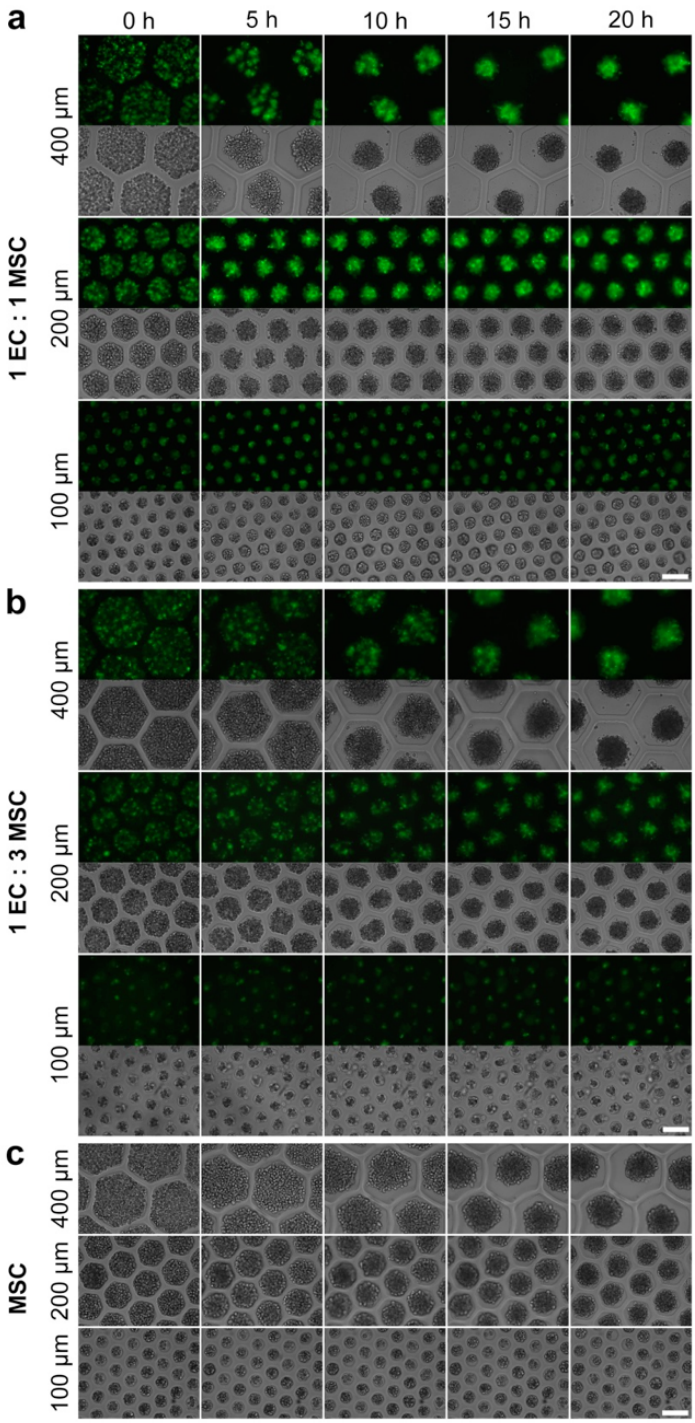

Figure S7. Initial phase of organoid formation and self-sorting. Related to Figure 4. Shown are the first 20 hours of self-assembly and self-sorting immediately after seeding GFP-HUVEC and hAMSC cell mixtures in alginate microwells (100, 200, 400 µm). Fluorescent and brightfield images were acquired with a 10x objective. Scale bars are 200 µm. **(A)** 1 HUVEC : 1 hAMSC organoids. **(B)** 1 HUVEC : 3 hAMSC organoids. **(C)** hAMSC only organoids.

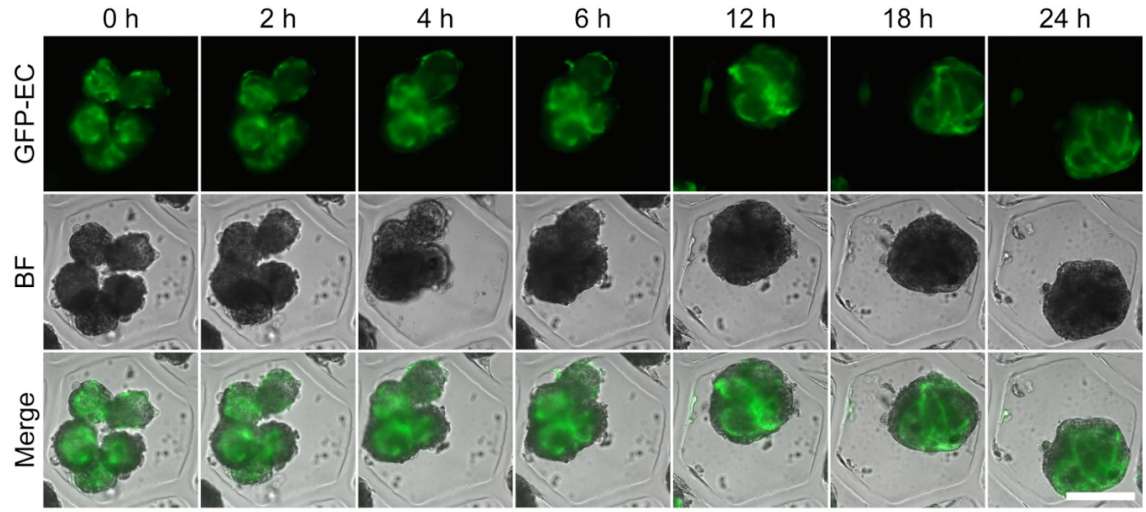

Figure S8. Organoid fusion to form macrotissue. Related to Figure 4. Organoids were created in 200 µm sized microwells at 1:1 and 1:3 GFP-HUVEC to hAMSC ratio. Organoids were cultured for 3 days in maintenance medium and 6 days in a vasculogenic medium to induce prevascularization (as seen at 0 h). For this assay the same vasculogenic medium was used. Prevascularized organoids were placed in a collagen-alginate microwell. GFP fluorescence and brightfield images were acquired with a 10x objective in time-lapse microscopy over 24 h. Scale bar is 200 µm.

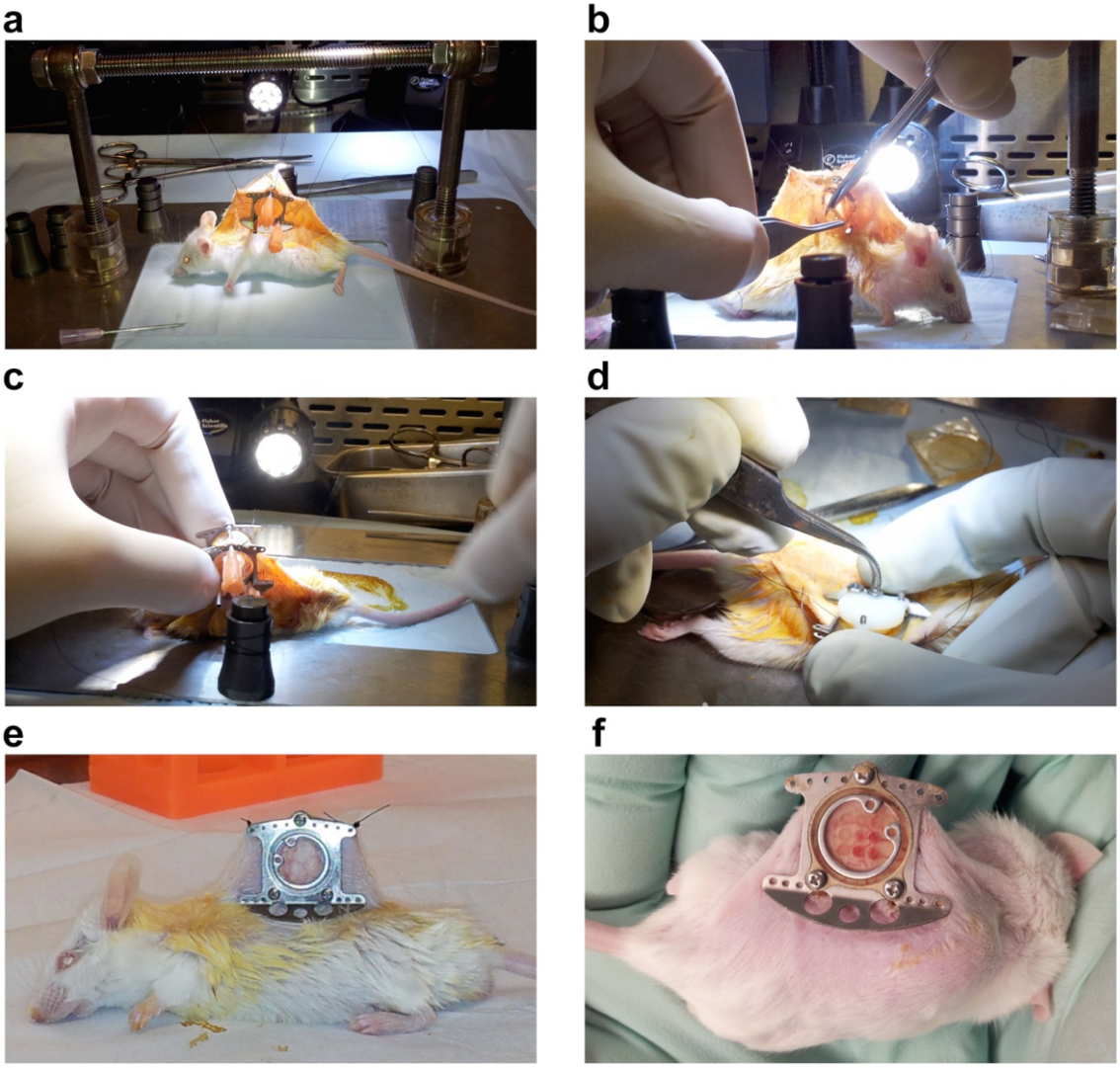

Figure S9. Window chamber surgery. Related to Figure 5. (A) Dorsal skin was spread out and backside of window chamber was connected. Needles were used to create holes for window chamber. (B) A circle was marked on the skin to indicate the opening for the window chamber and the skin was carefully cut out. (C) Front and back of window chamber were assembled. (D) Nuts were used to lock the window chamber. A custom 3D printed backing was used to hold the skin in place. (E) Closed window chamber in place; Secured with lateral sutures. (F) A custom-made window chamber insert to test up to 9 conditions simultaneously was included.

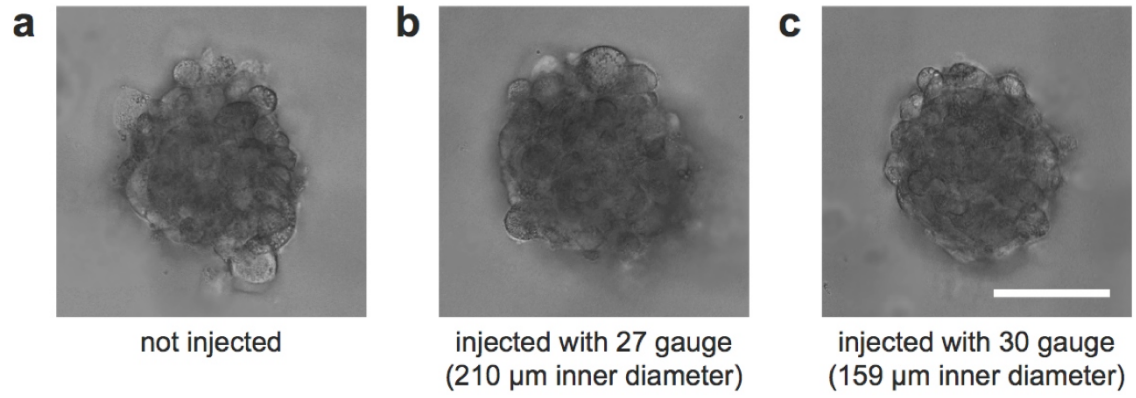

Figure S10: Robustness to shear stress. Related to Figure 5 and Figure 6. Images of organoids before (A) and after injection through a 27 gauge needle (B) and a 30 gauge needle (C). Scale bar is 50 µm.

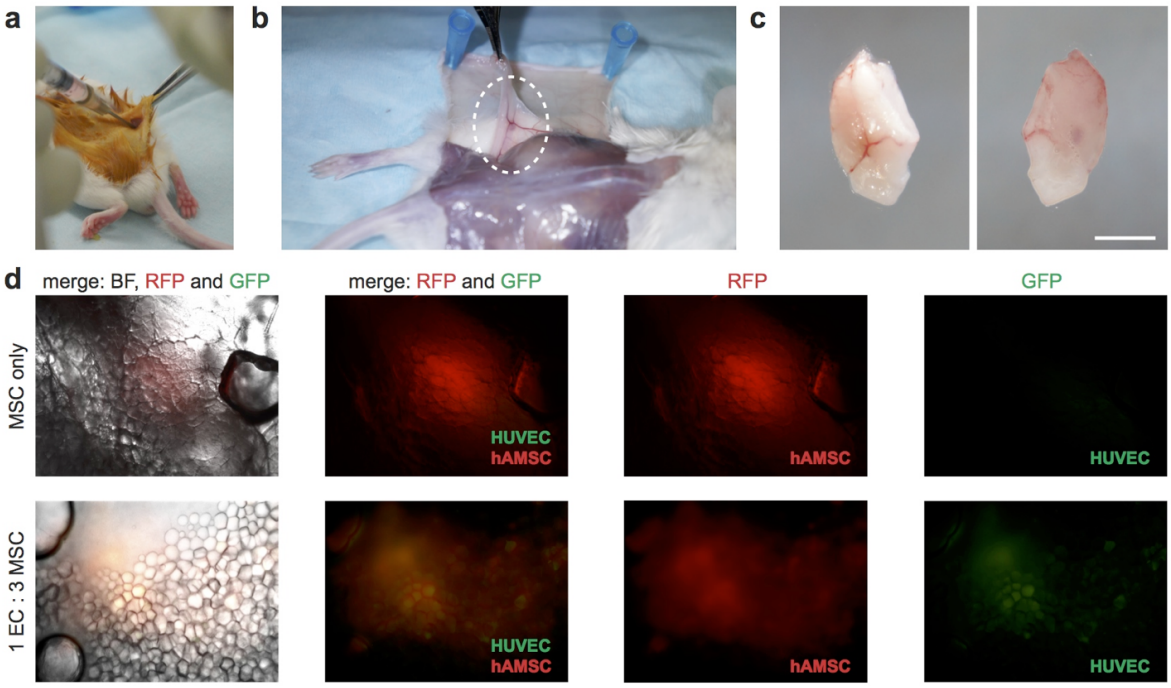

Figure S11. Procedure for injecting organoids *in vivo* (without window chamber). Related to Figure 5.
(A) Injecting a solution with organoids (1EC:3MSC and 200 μm size) into the adipose tissue of the obliques. A small incision along the back was made to ensure the correct position of the injection site. (B) The mice were sacrificed and the entire obliques (white dashed circle) were excised after 18 days of implantation. (C) Front and back of the extracted obliques. Scale bar is 2.5 mm. (D) Merged and individual images of brightfield and fluorescent images showing the position of the injected organoids. Top: RFP-MSC only organoids. Bottom: 1 GFP-ECs : 3 RFP-MSC ratio organoids. The organoids were composed of a 1 GFP-ECs : 3 RFP-MSCs ratio here due to the increased fluorescent signal from the RFP-MSCs, which facilitated imaging.

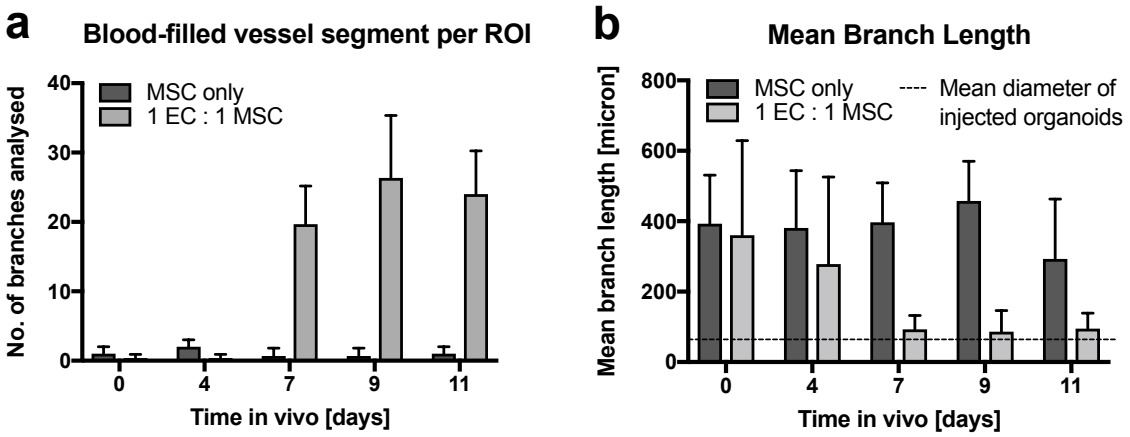

Figure S12. Additional quantification of the blood-filled vasculature formed in healthy mice upon injection of organoids as observed in real time via a window chamber. Related to Figure 5. (A) Quantification of the number of blood-filled vessel segments counted and measured to be accumulated into the total length of vasculature (Fig. 5c) within three ROI of 800-by-800 μm containing up to 60 blood-filled vessel branches. The number of blood-filled vessels increases substantially after day 7 for prevascularized organoids. There is no substantial difference in number of blood-filled vessels for the unvascularized organoids. (B) The mean length of the blood-filled vessel segments as the new vasculature is formed and integrated. The mean length of the blood-filled vessel segments decrease from the length of the large existing vessels in each ROI down to 93 ± 39 μm (day 7), 86 ± 29 μm (day 9), and 93 ± 44 μm (day 11) as the prevascularized organoids forms new vessels that connect with the host vasculature to become perfused and measurable. The distribution of branching length in the newly formed microvasculature day 7, 9 and 11 can be seen in Fig. 5d. There is no difference in mean length of the blood-filled vessels for the unvascularized organoids. As the new vessel formation in the ROI with injected prevascularized organoids becomes perfused and measurable on day 7, the mean length of the blood-filled vessel segments approach the mean diameter of the injected prevascularized organoids (71 ± 5 μm) denoted with a dashed line.

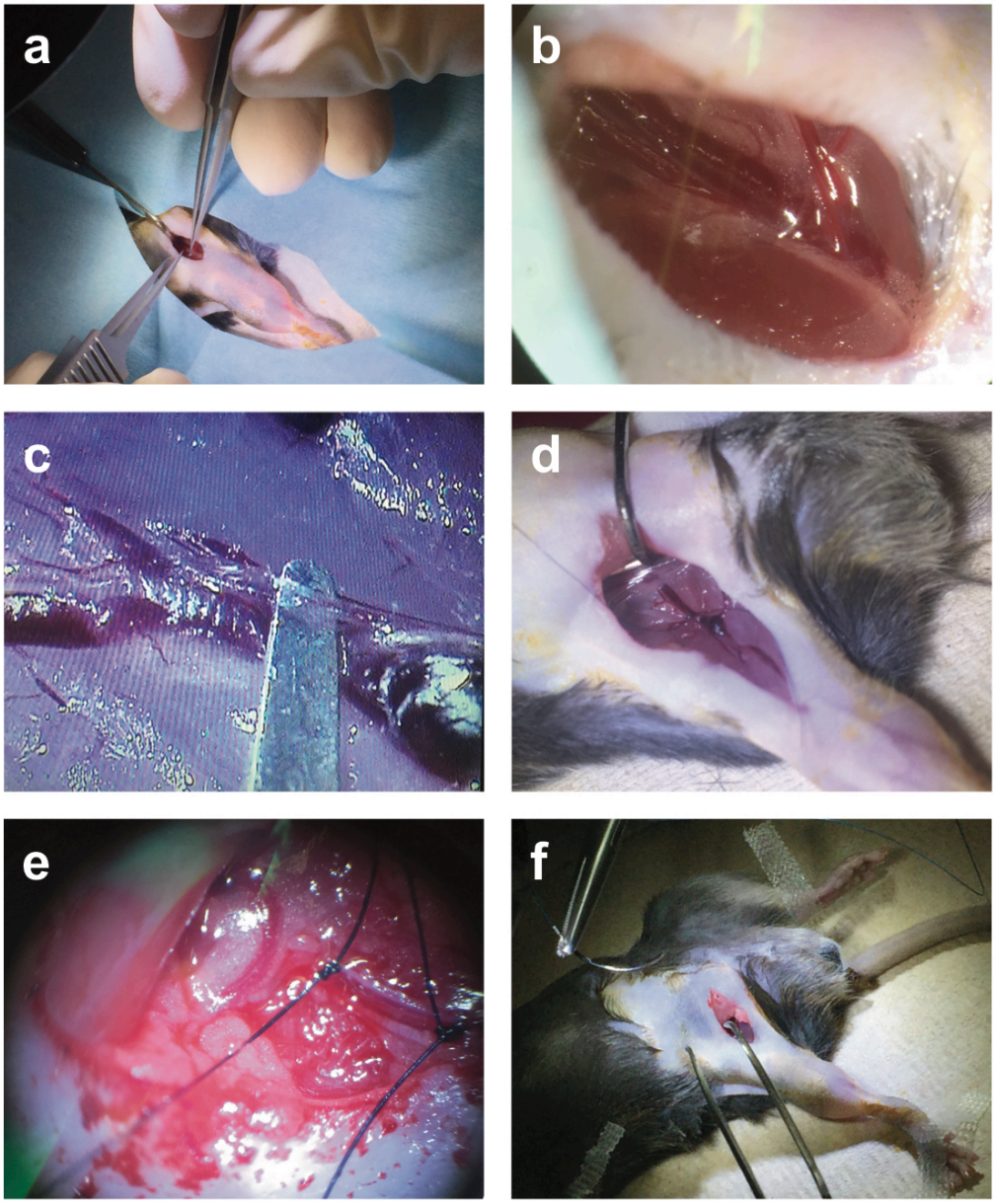

Figure S13. Surgical steps for modified induced hindlimb ischemia mouse model. Related to Figure 6.
(A) A skin incision was made over the femoral artery for a high femoral artery ligation and total excision as previously described (Brenes et al., 2012) . (B) Fascia was cleared and the femoral artery identified (picture taken through microscope). (C) The femoral artery was isolated from the femoral vein and nerve bundle (picture taken through microscope). (D) Sutures were inserted under the femoral artery and tied off (picture shows the first tie). (E) The femoral artery was doubly ligated and excised in its entirety. (F) The incision was closed.

Table S1. Table of advantages for different cell aggregation production methods, Related to Figure 2 and Figure 3

Cell Aggregate Production Method	High throughput	Output (no. of cell aggregates)	Easy automation (liquid handling in all steps)	Size control	Continuous observation	Easy harvesting	Biologically inert process suitable for *in vivo* use	Reference
Sacrificial hydrogel microwells	++	10,000s per mold	+	+	+	+	+	Current Study
Hanging drops	-	60 to 384 per culture plate	+	+	-	+	+	(Tung et al., 2011, Cavnar et al., 2014, Kelm et al., 2005)
Spinner culture	+	1,000s per spinner flask	+	-	-	+	+	(Sutherland et al., 1971)
Microwells	+	1,000s per mold	-	+	+	-	+ - (for PDMS microwells)	(De Moor et al., 2018, Dissanayaka et al., 2014, Liu et al., 2014, Lee et al., 2018, Jeong et al., 2016)
Non-adhesive 96 well plate	-	96 per culture plate	-	+	+	-	+	(Ehsan et al., 2014, Metzger et al., 2011, Wenger et al., 2005)

Table S2. Reproducibility and control of vascularized organoids, Related to Figure 3 and Figure 4

Reference	Method for producing vascularized organoids	Control over size in cited study	Structural organization of cells within organoid		Control over shape (circularity)	Organized vascular architecture within aggregates
			Observation of core-shell formation	Control over core-shell structure		
Current study	Sacrificial hydrogel microwells	Yes -by controlling size of alginate microwells	Yes	Yes -by changing presence of growth factors -by controlling ratio of ECs to MSCs	High	Present
(Kelm et al., 2005)	Hanging drop	Yes -by controlling cell number	Yes	Not demonstrated	High	Present
(De Moor et al., 2018)	Microwells	No	Yes	Not demonstrated	High	Present
(Wenger et al., 2005)	Non-adhesive 96 well plate	No	Yes	Not demonstrated	Medium	Absent
(Kim et al., 2019)	Thermoresponsive hydrogel sheets	Yes -by controlling size of hydrogel sheet	Yes	Yes -by controlling method of seeding cells on hydrogel surface -by controlling HUVEC cell density	Medium	Absent
(Tiruvannamalai Annamalai et al., 2016)	Cells embedded within gels	No	No	No	Low	Present

TRANSPARENT METHODS

Experimental design

The objective of this study was to develop an approach to form self-organized organoids in a scaleable and gentle manner, for use as an injectable cell therapy. As such, we designed dissolvable alginate microwells to culture organoids, promote self-organization of the cells, and gently harvest the organoids. We then demonstrated their functionality in two mouse models: a healthy mouse model using a window chamber, in a mouse model of hindlimb ischemia. All cells used in these studies were purchased commercially, all animal procedures were approved by the Columbia University Institutional Animal Care and Use Committee (IACUC) and all experiments were performed in accordance with relevant guidelines/regulations.

Fabrication of alginate microwells

We developed an experimental setup to culture cellular organoids with high throughput and without the labor-intensive hanging drop approach. We seed the cells onto an alginate construct with between 379 and 30,000 microwells. The cells will settle into these microwells, and as the alginate provides no adherence structure for the cells, the cells will adhere strongly to each other forming spherical cell aggregates over the initial 24 hours.

The alginate microwells are cast on hydrophilic PDMS molds. We fabricated master molds in SU-8 (SU-8 3050, Microchem, Newton, MA) on 3-inch Si wafers (Silicon Sense, Nashua, NH) by photolithography as described before (Gillette et al., 2011) to cast polydimethylsiloxane (PDMS, Sylgard 184, Essex Brownell, Fort Wayne, IN) replicas from the masters. We then made the PDMS molds hydrophilic by plasma treatment, and submerged them in distilled water to retain their hydrophilicity. We then autoclaved the PDMS molds prior to casting alginate.

We then prepared and autoclaved a 2% w/v alginate (Pronova UltraPure MVG, NovaMatrix, Drammen, Norway) or 7.5% w/v alginate (Alginic acid sodium salt, Millipore Sigma, St Louis, MO) in HEPES saline buffer solution (Ultrasaline A, Lonza, Basel, Switzerland). The alginate was pipetted into the PDMS molds. We used positive-displacement pipettes for accurate pipetting of viscous alginate solutions and to avoid bubbles. We closed the top of the molds with cellulose dialysis membranes (6000 Da MWCO), and flattened the membranes using the edge of a sterile glass slide. A 60 mM $CaCl_2$ HEPES buffer solution was pipetted on top of the membrane for at least 60 min to crosslink the alginate at room temperature. We removed the hydrogels from the molds using sterilized tools, and placed the hydrogels in HEPES saline buffer solution (Ultrasaline A, Lonza, Basel, Switzerland) supplemented with 1.8 mM $CaCl_2$ (to prevent leaching of the calcium ions from the hydrogels). We then transferred the alginate hydrogels into sterile culture ware, such as 24-well plates (Fisher Scientific, Fair Lawn, NJ) with the open micro wells facing up and stored them at 4°C until further use.

Uncrosslinking of sacrificial alginate

To determine the length of time required to uncrosslink the microwells, 7.5% w/v alginate microwells were fabricated as described in the previous section, and stored in 1.8mM $CaCl_2$ overnight. The following day, the alginate microwell scaffolds were transferred to preweighed, individually cut wells (from a 24 well plate), any excess $CaCl_2$ was removed, and the initial mass of the alginate scaffolds was measured. We then added 1 mL of PBS, 0.5% w/v sodium citrate, or 5% w/v sodium citrate to the well, and after 1 minute the excess supernatant was removed, the remaining alginate scaffold was weighed, and a fresh solution of PBS, 0.5% sodium citrate or 5% sodium citrate was added. This was repeated until the alginate microwell scaffold was fully uncrosslinked (by the sodium citrate).

Cell sources

GFP-labeled human umbilical vein endothelial cells (GFP-hUVECs) (Angioproteomie, MA, USA) were cultured in Endothelial Growth Medium 2 (PromoCell, Heidelberg, Germany). Adipose derived human mesenchymal stem cells (hAMSCs) (Promocell, Heidelberg, Germany) were cultured in Mesenchymal Stem Cell Growth Medium (Promocell, Heidelberg, Germany). Mouse endothelial cells (mECs) (Cell Biologics, IL, USA) were cultured in Complete Mouse Endothelial Cell Media (Cell Biologics, IL, USA). RFP-labeled mouse mesenchymal stem cells (RFP-mMSCs) (Cyagen, CA, USA) were cultured in DMEM with 10% FBS and 1% PenStrep (all from LifeTechnologies). All cells were gently passaged at 80-90% confluency using TrypLE (LifeTechnologies) and used only until passage P6 and mMSC until P8. Cells were cultured in 37°C and 5% CO_2-balanced, humidified atmosphere.

Fabrication of organoids

HUVECs and MSCs were harvested from 2D cell culture, counted and desired cell ratios of HUVECs to MSCs were prepared: MSC only, 1 HUVEC to 3 MSC, 1 HUVEC to 1 MSC and 3 HUVEC to 1 MSC, at a final concentration of $25x10^6$ total cells/mL.

Then the 1.8 mM $CaCl_2$ solution that the alginate microwells were stored in was removed, and replaced with DMEM (ATCC, Manassas, VA). The microwells were then placed in the incubator at 37°C and 5% CO_2 to equilibrate for at least 20 minutes. Then DMEM was removed and the microwell constructs gently dried using surgical spears (Braintree Scientific, Braintree, MA) leaving the microwell features covered.

20 µL of each cell suspension was then pipetted on to alginate molds in 24-well plate inserts with 100, 200 and 400 µm microwell size using a positive displacement pipette. Cells were left to settle to the bottom of the microwells for 20 minutes and the culture wells were then filled up with culture medium. This total cell number ($0.5x10^6$) was selected because it is appropriate for all three microwell sizes, in terms of even cell distribution, and the formation of a single organoid.

Culture media

The first 3-4 days after seeding, the cells were cultured in maintenance medium: Dulbecco's Modified Eagle Medium (DMEM) with 10% Fetal Bovine Serum (FBS) and 1% PenStrep (all from LifeTechnologies), with 50 µg/mL Sodium L-ascorbate (Sigma-Aldrich). For Fig. 4 and 5, the maintenance medium also included 20 mM Hepes (Fisher Scientific, Fair Lawn, NJ), 1 µM Insulin (LifeTechnologies, Carlsbad, CA), 250 nM T3, 1 µM dexamethasone, 0.5 mM IBMX, 50 µM Indomethacine, 1 µM Rosiglitazone and 1 µM CL316243 (all from Sigma, St. Louis, MO). After the first 3-4 days, the media was changed from maintenance medium to vasculogenic medium: Dulbecco's Modified Eagle Medium (DMEM) with 10% Fetal Bovine Serum (FBS) and 1% PenStrep (all from LifeTechnologies), with 50 µg/mL Sodium L-ascorbate (Sigma-Aldrich), 40 ng/mL bFGF and 40 ng/mL VEGF recombinant human protein (both from LifeTechnologies). For Fig. 4 and 5, the vasculogenic media also included 20 mM Hepes, 1 µM Insulin, and 250 nM T3. The cells were cultured in vasculogenic medium up to day 11. Cell media was changed every other day.

Harvesting of organoids

To collect organoids, the alginate hydrogel was uncrosslinked (Gillette et al., 2008). For this, the culture medium of the organoids was replaced with 5%w/v sodium citrate solution for approximately 20 min. This chelator liquefied the alginate, and allowed for resuspension of the organoids in a desired medium. Organoids were then centrifuged at 300 rpm for 5 minutes or as specified and the organoid pellet carefully collected for further use.

Organoid fusion

To test the ability of organoids to assemble *in vitro* and fuse to a larger tissue, 200 µm sized organoids of only hAMSCs, 1 EC : 3 hAMSC and 1 EC : 1 hAMSC ratio were placed in a 400 µm sized microwell of collagen-doped alginate (Gillette et al., 2011) composed of 3.5% collagen and 1%

alginate. These organoids had previously been prevascularized as described above. Organoid fusion was conducted in vasculogenic medium and observed for 24 hours.

Formation of macrotissue

To yield a large enough number of organoids in parallel to produce a macroscopic tissue, we seeded a co-culture of 1 MSC : 1 EC ratio onto an alginate microwell construct that fits into a 60 mm culture dish and produces over 30,000 organoids (Fig. 2a and c). The cells were cultured in maintenance medium without growth factors for 4 days with daily media change due to the high number of cells. The organoids were collected by removing the medium and uncrosslinking the alginate with 5 mL 5%w/v sodium citrate solution. The alginate liquefied and the organoid solution was gently collected, spun down and resuspended in 1 mL vasculogenic media. To facilitate sustained culture and imaging of the macro-tissue, we had constructed a 1 cm^2 cylindrical hole in a 1 cm thick 10% agarose layer in the middle of a 60 mm dish. The hole was made by placing a 1 cm^2 by 1 cm PDMS mold in the middle, pouring on agarose and removing the PDMS cylinder when the agarose had gelled. The 1 mL organoid suspension was pipetted into the hole, allowed to settle for 1 hour, and then had 5 mL vasculogenic media added on top. The media was changed daily.

Window chamber surgery

Organoids were collected as described above. The suspension was gently spun down at 220 g for 5 minutes. The supernatant was removed and the organoids resuspended in 200 µl PBS. In vitro created, prevascularized and non-prevascularized organoids were implanted in a window chamber to allow for continuous in vivo monitoring of the vascularization and integration process. Window chamber surgeries were conducted as described previously (Laschke et al., 2011, Palmer et al., 2012). A titanium window chamber (APJ Trading, Ventura, CA) was surgically implanted midline on the dorsum of male SCID mice (strain: ICRSC-M-M, 5-6 weeks of age, Taconic, Hudson, NY) after hair removal and ethanol and iodine disinfection.

To reduce variability between mice, prevascularized and non-prevascularized organoids were implanted in individual compartments of the same window chamber. Organoids were delivered by injection and pipetting underneath the fascia of connective tissue to the subcutaneous adipose tissue. Window chambers were closed with a circular glass cover slip and a retaining ring (APJ Trading, Ventura, CA). A custom-made 3D printed window chamber backing was attached to reduce skin movement in the window chamber. In a subset of experiments, a custom-made ultem plastic 9 well array was screwed onto the front frame of the window chamber to allow for high throughput in vivo testing. Here, organoids were placed into one of the 9 wells.

Animals were housed aseptically in frog cages to allow for enough clearance for the window chamber while still permitting easy access to standard laboratory chow (Irradiated globle rodent diet, Fisher Scientific, Fair Lawn, NJ) and drinking water ad libitum. Follow up buprenorphine administration (0.1mg/kg bodyweight) for pain management was given subcutaneously every 6-12 hours after surgery for the next 2 days post-OP. CO_2 euthanasia and cervical dislocation were performed after 30 days or earlier if necessary.

The animal procedures were approved and carried out in accordance to local regulations and authorities. The surgeries were conducted in aseptic technique.

Hindlimb ischemia surgery

Hindlimb ischemia-inducing surgeries were conducted as described previously (Brenes et al., 2012). Briefly, ischemia was induced in the right hindlimb of the mouse by a high femoral artery ligation and total excision of the superficial femoral artery in 20 week-old C57BL/6 mice (The Jackson Laboratory, Bar Harbor, ME). Mice were anesthetized with isoflurane and maintained on a warmed surface. Intraperitoneal injection of buprenorphine, for analgesia, and ultrasaline, for increased hydration, were administered pre-operatively. Mice were positioned in dorsal recumbency with their

hindlimbs externally rotated. Lidocaine, for local anesthesia, was administered subcutaneously at the shaven surgical site, which was subsequently sterilized with ethanol and iodine. A skin incision was made over the femoral artery beginning at the inguinal ligament and continued caudally to the popliteal bifurcation. The femoral artery was isolated from the femoral vein and nerve bundle, and the femoral artery was doubly ligated and excised from the distal site of the deep femoral artery bifurcation to the saphenous and popliteal bifurcation. Prevascularized organoids (corresponding to a total of $2x10^6$ cells) or control medium at a volume of 0.1 mL were injected into the semimembranosus muscle at four sites along the thigh, immediately following femoral artery ligation and the incision was closed with 4-0 nylon suture. The prevascularized organoids were made in 200 µm micro wells from a 1 RFP-mMSCs : 1 mECs mix. Body temperature was maintained with heating pads until the animals recovered from surgery and were ambulatory. Animals were housed separately and closely monitored.

The animal procedures were approved and carried out in accordance to local regulations and authorities. The surgeries were conducted in aseptic technique.

Laser speckle contrast imaging (LSCI) to measure perfusion

Laser speckle contrast imaging (LSCI) was used to measure perfusion of the ligated and naïve limbs on Day 0, 1, 2, 3, 5, 7, 9, 11 and 14 post-surgery. A LSCI system was build (Ponticorvo and Dunn, 2010) and consisted of a 810 nm infrared laser diode, a beam expander and a CCD camera with a band-pass filter. The mice were briefly anesthetized with isoflurane and placed in sternal recumbency with the hindlimb stretched out behind them exposing the plantar surface of the hind paws. For each measurement, 40 consecutive images were obtained and the spatial speckle contrast was estimated from a 7x7 window of pixels (Boas and Dunn, 2010). Average hind limb perfusion was determined for an anatomical defined region of the foot – the plantar surface of the hind paw spanning the digital, metacarpal and carpal pads. Calculated perfusion was expressed as a ratio of the mean perfusion of the planter surface of the right (ischemic) to the left (control) hind limb.

Histological analysis

The animals were euthanized 14 days after femoral artery ligation. The bilateral gastrocnemius muscle from both hindlimbs were fixed, paraffin-embedded, cross-sectionally sliced and stained for H&E. The total number of myofibers were counted and the percentage distribution of regenerating (centralized nuclei), viable (striated) and necrotic (broken swollen pale hyalinized) myofibers were calculated for at least three ROI.

Imaging

A Leica DMI 6000B inverted microscope with 4x and 10x objectives, equipped with a motorized stage (Leica Microsystems, Bannockburn, IL) and a QImaging Retiga 2000R monochrome camera (QImaging, Surrey BC, Canada) was used to acquire fluorescence and brightfield images. Leica LAS X software was used for image acquisition. Cropping, color adjustments and contrast enhancements of images as well as Z-stack projections were performed in ImageJ. For time lapse imaging of organoid formation and organoid fusion an environmental chamber was used to maintain 37°C and 5% CO_2. Images were acquired every 30min.

Confocal images of the window chamber were taken using a Leica SP5 confocal system with a 10.0x 0.30 N.A. objective. To be able to image the window chamber mice were anesthetized with isoflurane. Due to the stressfulness of the anesthesia of the imaging procedure, in vivo images were acquired every 2-3 days.

To precisely observe individual organoids, we took stacks of confocal images (1024x1024 pixels, 41 images with a z- spacing of 0.25 microns) using a Leica SP5 confocal microscope, with a 100x 1.43 N.A. oil immersion objective (Leica Microsystems) at a resolution of 0.132 µm/pixel (image stacks were thus 135 mm * 135 mm * 10 mm). We simultaneously collected the differential interference contrast (DIC) images as well as the RFP- and GFP-signal.

Statistical analysis

One-way ANOVA with Bonferroni's *post hoc* tests was performed using Graphpad Prism 7 software.

References

BOAS, D. A. & DUNN, A. K. 2010. Laser speckle contrast imaging in biomedical optics. *J Biomed Opt,* 15**,** 011109.

BRENES, R. A., JADLOWIEC, C. C., BEAR, M., HASHIM, P., PROTACK, C. D., LI, X., LV, W., COLLINS, M. J. & DARDIK, A. 2012. Toward a mouse model of hind limb ischemia to test therapeutic angiogenesis. *J Vasc Surg,* 56**,** 1669-79; discussion 1679.

CAVNAR, S. P., SALOMONSSON, E., LUKER, K. E., LUKER, G. D. & TAKAYAMA, S. 2014. Transfer, imaging, and analysis plate for facile handling of 384 hanging drop 3D tissue spheroids. *J. Lab. Autom.,* 19**,** 208-214.

DE MOOR, L., MEROVCI, I., BAETENS, S., VERSTRAETEN, J., KOWALSKA, P., KRYSKO, D. V., DE VOS, W. H. & DECLERCQ, H. 2018. High-throughput fabrication of vascularized spheroids for bioprinting. *Biofabrication,* 10**,** 035009.

DISSANAYAKA, W. L., ZHU, L., HARGREAVES, K. M., JIN, L. & ZHANG, C. 2014. Scaffold-free Prevascularized Microtissue Spheroids for Pulp Regeneration. *J Dent Res,* 93**,** 1296-303.

EHSAN, S. M., WELCH-REARDON, K. M., WATERMAN, M. L., HUGHES, C. C. & GEORGE, S. C. 2014. A three-dimensional in vitro model of tumor cell intravasation. *Integr Biol (Camb),* 6**,** 603-10.

GILLETTE, B. M., JENSEN, J. A., TANG, B., YANG, G. J., BAZARGAN-LARI, A., ZHONG, M. & SIA, S. K. 2008. In situ collagen assembly for integrating microfabricated three-dimensional cell-seeded matrices. *Nat. Mater.,* 7**,** 636-40.

GILLETTE, B. M., ROSSEN, N. S., DAS, N., LEONG, D., WANG, M., DUGAR, A. & SIA, S. K. 2011. Engineering extracellular matrix structure in 3D multiphase tissues. *Biomaterials,* 32**,** 8067-76.

JEONG, G. S., NO DA, Y., LEE, J., YOON, J., CHUNG, S. & LEE, S. H. 2016. Viscoelastic lithography for fabricating self-organizing soft micro-honeycomb structures with ultra-high aspect ratios. *Nat. Commun.,* 7**,** 11269.

KELM, J. M., SANCHEZ-BUSTAMANTE, C. D., EHLER, E., HOERSTRUP, S. P., DJONOV, V., ITTNER, L. & FUSSENEGGER, M. 2005. VEGF profiling and angiogenesis in human microtissues. *J. Biotechnol.,* 118**,** 213-229.

KIM, E. M., LEE, Y. B., KIM, S.-J., PARK, J., LEE, J., KIM, S. W., PARK, H. & SHIN, H. 2019. Fabrication of core-shell spheroids as building blocks for engineering 3D complex vascularized tissue. *Acta Biomater.*

LASCHKE, M. W., VOLLMAR, B. & MENGER, M. D. 2011. The dorsal skinfold chamber: window into the dynamic interaction of biomaterials with their surrounding host tissue. *Eur Cell Mater,* 22**,** 147-64; discussion 164-7.

LEE, J. M., YANG, L., KIM, E.-J., AHRBERG, C. D., LEE, K.-B. & CHUNG, B. G. 2018. Generation of uniform-sized multicellular tumor spheroids using hydrogel microwells for advanced drug screening. *Sci Rep,* 8**,** 17145.

LIU, T., WINTER, M. & THIERRY, B. 2014. Quasi-spherical microwells on superhydrophobic substrates for long term culture of multicellular spheroids and high throughput assays. *Biomaterials,* 35**,** 6060-6068.

METZGER, W., SOSSONG, D., BACHLE, A., PUTZ, N., WENNEMUTH, G., POHLEMANN, T. & OBERRINGER, M. 2011. The liquid overlay technique is the key to formation of co-culture spheroids consisting of primary osteoblasts, fibroblasts and endothelial cells. *Cytotherapy,* 13**,** 1000-12.

PALMER, G. M., FONTANELLA, A. N., SHAN, S. & DEWHIRST, M. W. 2012. High-resolution in vivo imaging of fluorescent proteins using window chamber models. *Methods Mol Biol,* 872**,** 31-50.

PONTICORVO, A. & DUNN, A. K. 2010. How to build a Laser Speckle Contrast Imaging (LSCI) system to monitor blood flow. *J. Vis. Exp.*

SUTHERLAND, R. M., MCCREDIE, J. A. & INCH, W. R. 1971. Growth of multicell spheroids in tissue culture as a model of nodular carcinomas. *J Natl Cancer Inst,* 46**,** 113-20.

TIRUVANNAMALAI ANNAMALAI, R., RIOJA, A. Y., PUTNAM, A. J. & STEGEMANN, J. P. 2016. Vascular network formation by human microvascular endothelial cells in modular fibrin microtissues. *ACS Biomater Sci Eng.,* 2**,** 1914-1925.

TUNG, Y. C., HSIAO, A. Y., ALLEN, S. G., TORISAWA, Y. S., HO, M. & TAKAYAMA, S. 2011. High-throughput 3D spheroid culture and drug testing using a 384 hanging drop array. *Analyst,* 136**,** 473-8.

WENGER, A., KOWALEWSKI, N., STAHL, A., MEHLHORN, A. T., SCHMAL, H., STARK, G. B. & FINKENZELLER, G. 2005. Development and characterization of a spheroidal coculture model of endothelial cells and fibroblasts for improving angiogenesis in tissue engineering. *Cells Tissues Organs,* 181**,** 80-8.